VRIJE UNIVERSITEIT BRUSSEL

UNIVERSITEIT GENT

Optimisation of the Finite Helical Axis estimation and its application in cervical kinematics

Master thesis submitted in order to be awarded the degree in
Master of Science in Biomedical Engineering

Violeta Yolanda Portero López

Academic year 2018-2019

Promotor: Prof. Erik Cattryse

Copromotor: Luca Buzzati

Abstract

Finite Helical Axis – Cervical Movement – Rotation motion – Kinematics – Error prone optimization

Although 6 DOF approach to analysis human movement is widely used among clinicians, it introduces problems in the reliability of the results due to the chosen reference dependence. The FHA approach solves this dependence problem since the parameters that describe its variability do not depends on the position and orientation in space relative to the chosen reference. However, it struggles with calculation error owing to the methodology used to obtain it. A rotating object simulation was performed in order to optimize the FHA estimation and find the algorithm with the least error prone. Single Value Decomposition was chosen as the most consistent method for FHA calculation after evaluating the error at different displacements. A head movement simulation performed in MATLAB was used to evaluate the effect of angle interval and adding noise on FHA error. The results of the simulation show proportional inversely between angle interval and FHA error, and a greater influence of orientation noise than position noise on FHA error. The optimisation of FHA estimations makes the FHA approach a method with less error prone which analyses with greater reliability human movement through the parameters that describe its dispersion.

Contents

List of figures

List of tables

List of Abbreviations

CNP	Chronic Neck Pain
CH	Convex Hull
FHA	Finite Helical Axis
HA	Helical axis
IHA	Instantaneous Helical Axis
MA	Mean Angle
MD	Mean Distance
RM	Rotation Matrix
ROM	Range of Motion
SVD	Single Value Decomposition

Chapter 1

1. Introduction

1.1. Clinical background

Through the study of human movement, functional analysis of the body can be evaluated, and the knowledge acquired contributes to a better diagnosis and treatment that improves quality of life. Human movement is a complex system integrated by different muscles, bones, ligaments and joints which interact with each other. Understanding the biomechanics of each joint is useful for clinicians in order to study disease etiology and detect injuries more accurately to give the best possible treatment options [1]. Kinematic knowledge is important for diagnosis and treatment of joint diseases since it is possible to understand human movement and propose models to simulate it, which is also a basis for the design of prosthesis.

Kinematics is the study of motion independent of the underlying forces that produce that motion. It includes position, velocity and acceleration which are all geometrical and time-related properties of motion, in contrast with dynamics, which specifies the causes of motion.

It is possible to evaluate human movement in vivo with accurate devices that capture the motion [2]. Currently, there are three main techniques for motion capture, among which we can find optical systems as photogrammetry, electromagnetic systems and inertial systems. Those systems record and analyze the movement in three dimensions with very high accuracy, using markers attached to the body. With these devices, human movement is sampled many times per second by the tracking system, and analyzed using a computer.

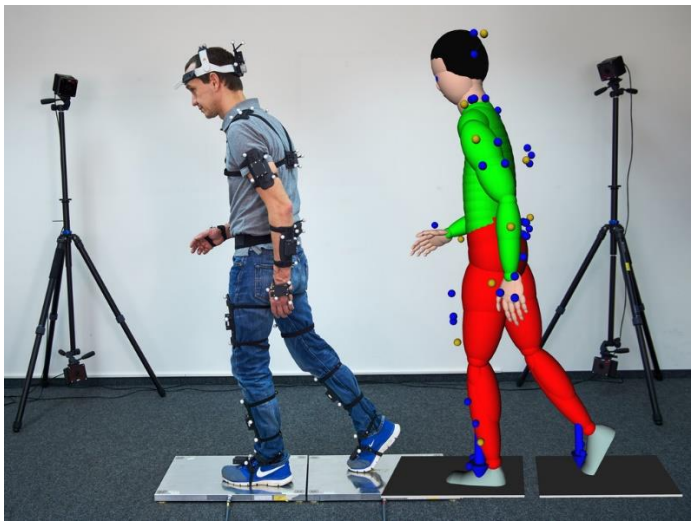

Figure 1-1: Motion capture with Advanced Realtime Tracking -Human. Image adapted from [3]

This type of tracking system can capture position, velocity, angle and acceleration of body segments and joints during motion. The variables obtained with the 3D tracking system (e.g. position, orientation, velocity) must be analyzed further in order to characterize the movement. For that purpose, a wide number of methodologies for kinematic analysis have been developed and will be evaluated in this section.

In general, kinematic analysis of human motion can be divided into two main groups. The first depicts the movement of the segments of the limbs interconnected by joints, where the relative rotation is described by the Euler angle system (Figure 1-2). This method requires a correct selection of the rotation axes between two bone segments. The second group analyzes in detail joint motion by describing rotation and translation using the helical axis (Figure 1-3). Knowing the surface geometry, the joint motion can be evaluated to obtain information concerning wear studies [4].

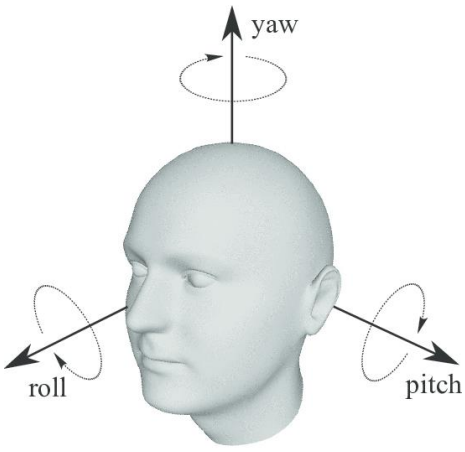

Figure 1-2: Six degrees of freedom approach: translation if three perpendicular axes combined with rotation about these axes, often termed pitch, yaw, and roll. Image adapted from [5]

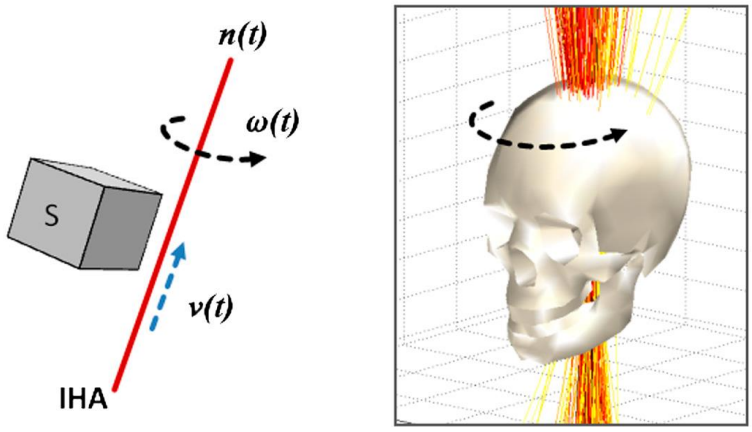

Figure 1-3: Representation of helical axis of an object. Image adapted from [6]

The most common method in human analysis is the six degrees of freedom (6 DOF) approach due to the ease of interpretation by clinicians. DOF of an articulated structure is the number of independent position variables necessary to specify the state of the structure. Six DOF is characterized by three translations along the axis and three rotations around them. Euler angle system is used to characterize rotation around the angles and consequently the orientation of the object in the space [9]. The Euler convention uses three rotations around two axes, being the first and third rotation axes the same (e.g. XYX). A variation of Euler angles is the so-called Cardan angles, which use three consecutive rotations around three axes (e.g. XYZ). The axes are fixed in the space and the final orientation depends on the sequence chosen.

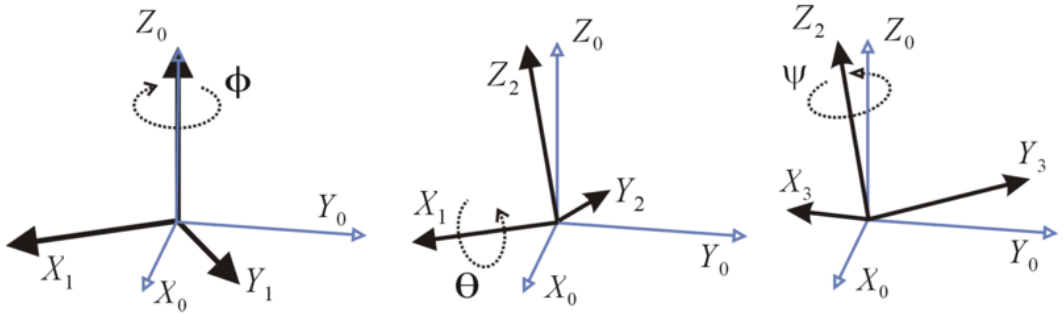

Figure 1-4: Euler angles: rotation sequence ZX'Z'

Parameters such as range of motion (ROM), angular velocity and jerkiness are used for the analysis of joint movement, as they characterize the state of the joint. Each joint has its own ROM (measured in degrees) and this depends on factors such as pain, stiffness and swelling in joints. Injuries may have effects on ROM of the joint. For a reliable comparison of ROM between patients, the same coordinate system must be used since it defines the amount of rotation around an axis.

The axis of rotation is a line oriented perpendicular to the plane in which the rotation occurs [12]. Angular velocity describes the rate of velocity at which an object is rotating around that axis. It has been reported in previous studies that injuries such as chronic neck pain leads to a reduced ROM and peak velocity of neck movements [13]. Those patients

may also present altered patterns of movement with an increase in irregularity which is related to impairment of motor control. Loss of motor control is also related with the concept of jerkiness. It involves fast movements which the patient cannot control, and it interrupts their normal movement.

Kinematic analysis plays an important role since with the different methodologies the specific parameters that characterize joint movement can be obtained and they could be easily interpreted by clinicians.

1.2. Problem statement: motion analysis in clinical biomechanics

Most of the problems of motion analysis are related to the chosen coordinates system, the anatomical location of the marker during the movement registration and the data analysis and parameters obtained to characterize the motion. That is why rigorous methods concerning to these issues are required.

Although 6 DOF is the most common approach between clinicians due to the facility of interpretation, it introduces problems in the reliability of the results while comparing between patients. The chosen coordinates system depends on the experiment conditions for each movement registration. It is difficult to replicate the same conditions for different patients since the reference system of the motion capture system can be in a different position as well as the posture of the patient. The predefined axes mostly do not reflect the rotation axes of the joint. This effect may lead to an over- or underestimation of angle values, called the “crosstalk effect” [16].

Particularly, cervical movement consists of the relative movement of the neck respect to the thorax/trunk, therefore small movements of the shoulder may lead to incorrect values for neck shift while using a fixed reference system.

To solve this problem, many authors define a reference system for each joint based on anatomical points to create a rotation matrix in order to change the reference (change of basis) [14]. Anatomical axis systems are based on anatomical landmarks in the skeletal geometry (Figure 1-5 and Figure 1-6).

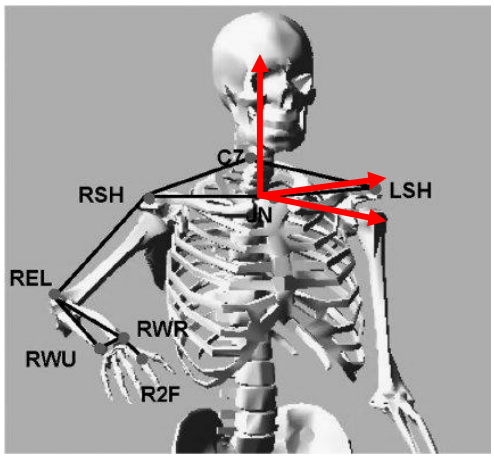

Figure 1-5: Anatomical landmarks: spinous process of the seventh cervical vertebrae (C7), the jugular notch where the clavicles meet the sternum (CLAV), the left and right acromio-clavicular joint (LSHO, RSHO), the right lateral epicondyle approximating the elbow joint axis (RELB), the right wrist bar thumb side (RWRA), the right wrist bar pinkie side (RWRB), and the dorsum of the right hand below the head of the second metacarpal (RFIN). Image adapted from [15]

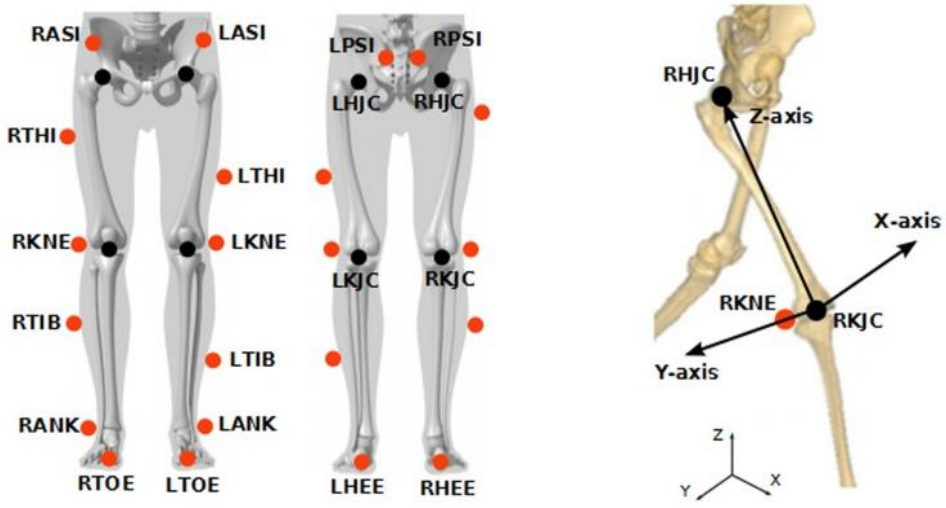

Figure 1-6: Knee coordinates system. Image adapted from [18]

Although resulting in an improved replication of conditions for different experiments, this method still presents problems in terms on finding the same anatomical points for different patients. Detection of these points requires a certain level of anatomical knowledge and problems of accuracy are introduced with the thickness of the soft tissue and error based on skin motion [22], the so called skin artefacts.

The difficulty in replication of the same experimental conditions between patients does not permit a reliable intra-session comparison since axes where rotations and translations are performed can be in different positions and orientation for different patients. Furthermore, the Euler angles approach has limitations, since there are different possible sequences and the final orientation of the object depends on the chosen sequence. In fact, for each of the three Cardan and Euler angles exist six different possible sequences [16]. Previous studies have reported the effect of altering the Euler angles sequence of rotation, noting difference up to 50 degrees for some angles [17].

Finite Helical Axis (FHA) solves the problem of coordinate system replication, since the parameters that describe its variability do not depend on the chosen reference. With the FHA approach, the rigid body movement is defined by a rotation around the axis and a translation along it [10] (Figure 1-7). This movement description covers all six degrees of freedom of the three-dimensional rigid-body movement but in contrast with the Euler approach it does not depend on any reference system as it constitutes the actual axis of motion of the joint [16].

Helical axis was investigated in previous studies from three-dimensional discrete kinematics to characterize human movement and has been suggested for analyzing joint kinematics of the foot, wrist, foot and cervical spine [7]. Many authors have used the FHA in their methodology and different algorithms were found for the calculation, but no comparisons between the different algorithms for HA estimation have been found. Despite the ability to overcome dependence on the chosen coordinate system, FHA struggles with problems related with calculation error and poor visualization techniques [16]. The stochastic error is inversely proportional to the displacement between the final position and the initial position.

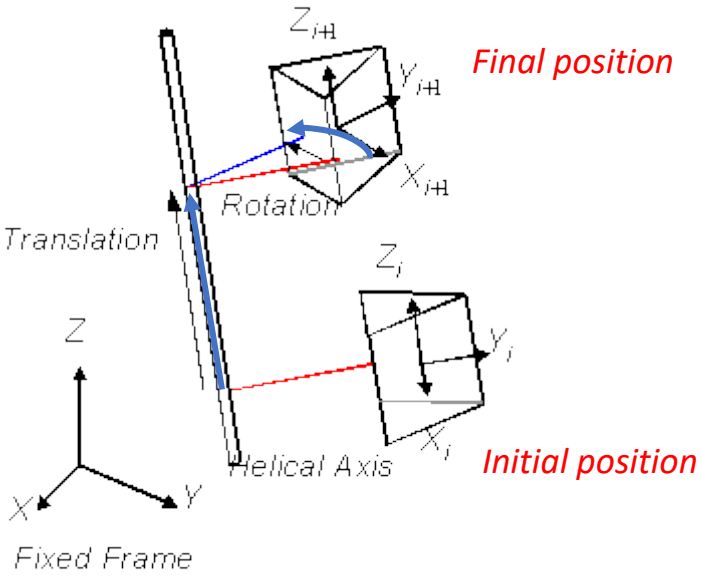

Figure 1-7: FHA represented by a rotation around the axis and a translation around it from the initial position to the final position. Image adapted from [19]

However, the human motion is considered a continuous movement such that the displacement over which the helical axes are calculated should be as small as possible. For that case, calculation error on the axis is characterized by small deterministic error but large stochastic errors [16]. Influence of displacement on FHA error was reported by other authors [6] but no comparison between the error introduced by different algorithms has been found in the literature for cervical movement. Other authors compared in their simulation more than one algorithm for the FHA but without any application in cervical kinematics [20].

Difficulties in interpreting FHA by clinicians is mainly due to the lack of user-friendly software capable of obtaining the characteristic parameters of FHA for a human movement. Many authors have developed parameters that characterize FHA axis behavior in cervical motion such as convex hull and mean angle [30][21], but any free interface has been created in order to analyze FHA behavior from patient motion data that can be used by the clinician to make diagnostic and treatment decisions.

1.3. Finite Helical Axis

Kinematically, joint movement may be defined at any time by its translation and rotation [6]. The movement of a joint segment can be considered as a series of finite displacements. In this case the movement is characterized by an angle of rotation around and a quantity of translation along an axis (Figure 1-7). This axis is called finite helical axis (FHA), due to the discretization of the movement into a series of displacements. Conversely, by taking the continuity of the movement into account, this movement will be characterized by a rotational speed (angular velocity) around and a translation speed along an axis defined by its instantaneous position and orientation in space. In this case, the axis is called Instantaneous Helical Axis (IHA) [20]. FHA axis coincides with IHA if the displacement is very small or if the axis is fixed, which is not the case for human joints. For the calculation of the FHA, it is required to know the initial and final position (displacement) of at least three points of the rigid body in order to know its orientation in space. The FHA can also be calculated with one point and its corresponding rotation matrix which provides information about the orientation of the point in space. These displacements during a movement can be expressed by rotation matrices (Figure 1-8). That matrix is used to perform a rotation in space, and it has an essential role in the calculation algorithm of the FHA.

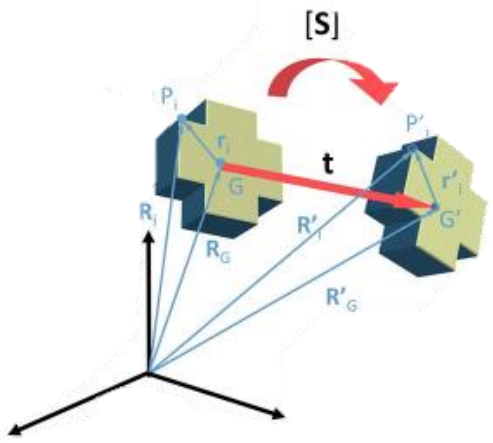

Figure 1-8: rotation of an object based on rotation matrix. Image adapted from [25]

$$R_i' = R_G + t + [S] \times r_i \quad (1)$$

P_i and P_i' are the initial and final position of the point (sensor). By clearing equation (1), the rotation matrix for the displacement is calculated.

The HA is perpendicular to the plane in which the rotation occurs. There are three types of so called planar head movements depending on the axis of rotation (Figure 1-9). The direction of that axis of rotation changes during the movement, as well as the position of a point in the axis. So that, it is important to estimate their value in order to make a reliable analysis. The superimposed helical axes are the results of the patient motion analysis.

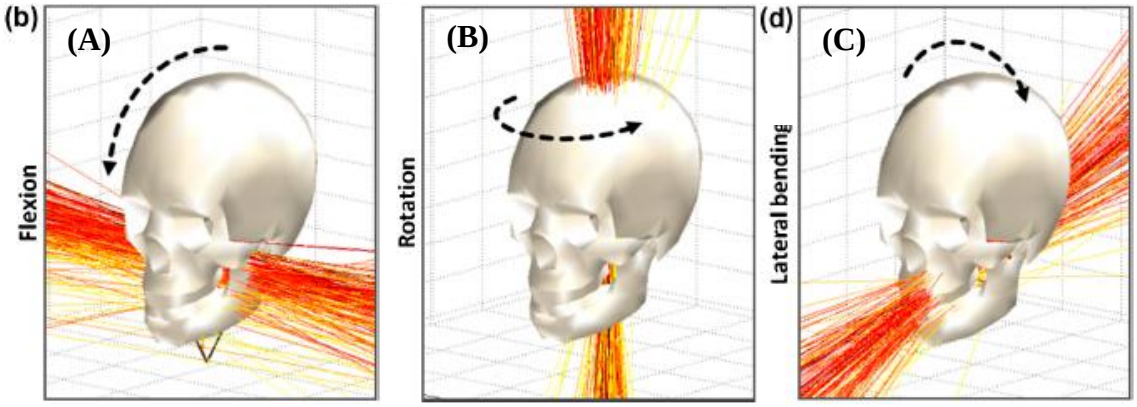

Figure 1-9: Head movements: flexion-extension (A), rotation (B) and lateral bending (C). Image adapted from [6]

For the FHA, the number of axes will depend on the head displacement chosen for its calculation. In other words, for the same motion sample, the number of FHA is higher if the displacement is smaller. The displacement is the path between the initial position and the final position for which one FHA is calculated. The entire movement will be divided in finite displacements for the calculation of all FHAs, which will characterize the motion of the patient. For a clinician, the displacement (called angle step) for the FHA calculation is very important, and its size can lead to different interpretations. A large angle step gives more general information about how the patient moves. It is more focused on determining the axis direction tendency for the whole movement, what can be called the axis of the movement. Contrarily, a small angle step gives information about the fluency and smoothness of the movement, which will be useful for a clinician to detect anomalies in the motion behavior of the joint. Evaluating the dispersion of these FHA values can provide information about joint functioning and decrease of motor control. A recent study on shoulder movements has found that young subjects showed significant lower helical axes dispersion compared to elderly subjects, as well as helical axes dispersion being smaller in the dominant arm with respect to the contralateral arm [23].

Focusing attention on cervical kinematics, it can be said that computation of movement axis is a determinant parameter for calculating the quality of motion owing to the relation between neck pain and irregularities of movement axis in respect of its location and orientation. The variability of the helical axis during active cervical movement were studied by other authors by comparing HA parameters, such as mean angle (MA) and mean distance (MD), between patients with chronic neck pain and asymptomatic people [24]. The results indicate less variable movement for those with neck pain relative to the control group. Figure 1-10 shows a higher dispersion of the angles of each HA, as well

as a higher dispersion in the position of the axes. The results for this study coincide with the shoulder study [23] and confirm the effectiveness of using HA approach in the clinical field.

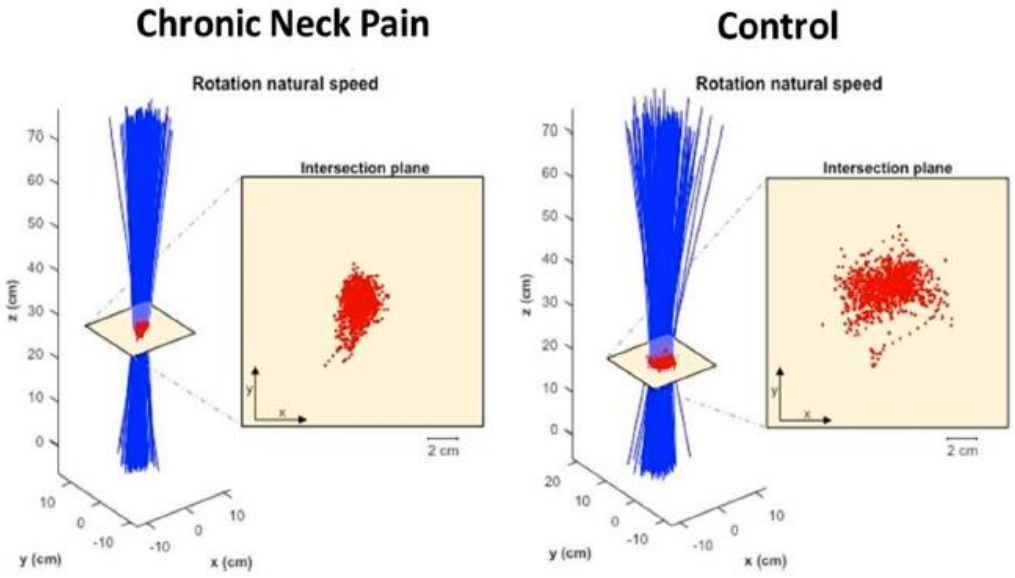

Figure 1-10: HA behavior from a patient and control subject during head rotation. Image adapted from [24]

Chapter 2

2. State-of-the-art

Some researchers have studied the potential for HA patterns to be used as a biomarker. A spinal health study evaluated parameters such as mean and standard deviation of HA vector orientation and center of rotation position among different patients in order to determine if HA approach may have an important role in disc health assessment [26]. The results for lateral bending movement showed that the orientation and standard deviation of HA near the neutral zone (moment = 0 Nm) were similar for healthy subjects and patients with spinal degeneration, and differences between these two parameters became accentuated at the end ranges of motion where degeneration severity increases the out-of-plane rotations and standard deviation of orientation, indicators of instability. For this study, the average HA orientation for the entire pathway of motion was calculated.

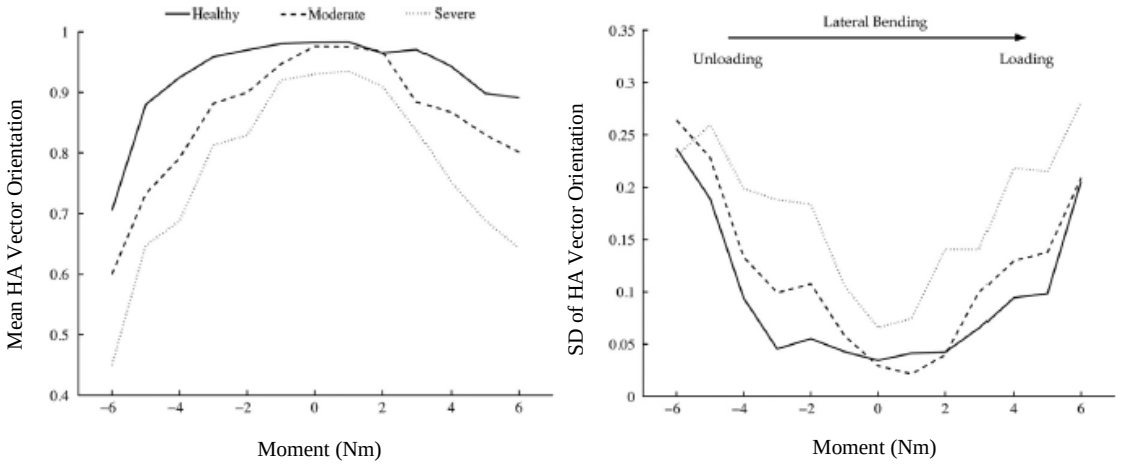

Figure 2-1: HA orientation and standard deviation. Three HA patterns are displayed: healthy, moderate degeneration and severe degeneration. X-axis represents the range of motion during lateral bending movement. Image adapted from [26]

Venegas et al. [31] averaged the cycles and normalized the time scale. Furthermore, parts where the angular speed was very small were removed. (where the displacement was so small that the resulting HA could not be calculated with accuracy). In this way, neck movement is associated with a curve. The aim of this study was to improve the inter-session reliability. Figure 2-2 shows the HA axoid position during three head flexion movements. Curves describe a coordinated movement of the cervical vertebrae.

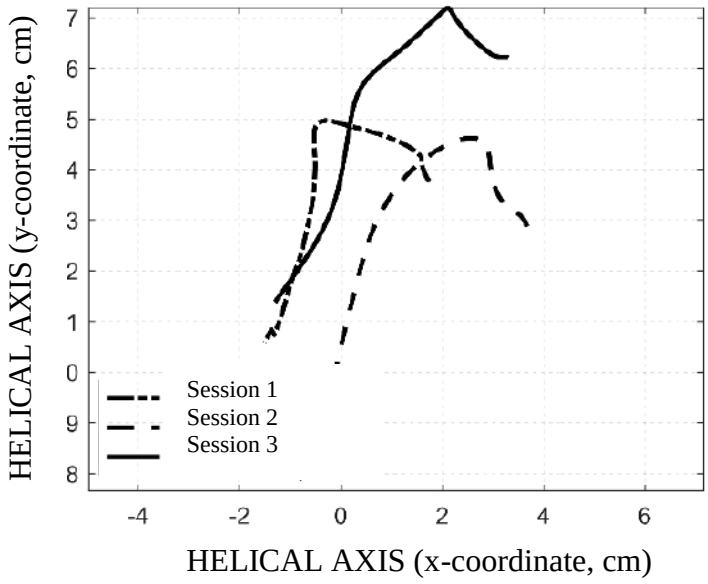

Figure 2-2: Mean HA behavior in the sagittal plane for the three sessions of a single subject in the flexion movement. Image adapted from [31]

Other studies opted to divide the whole movement into steps and calculate the HA for each step. Cescon et al. [6] calculated the mean vector orientation by averaging all HAs. This approach is different from the one explained above which averaged the cycles and then calculated the HAs in the mean cycle. In this study, the intersection points between the HAs and a set of planes perpendicular to the mean HA are calculated and analyzed using the convex hull technique. Finally, the minimum area is identified (Figure 2-3). The second metric used to quantify HA behavior in this research is the angle between the HA_0 and each of the HAs. Mean value of the distribution of such angles is computed and used as a metric (Figure 2-4).

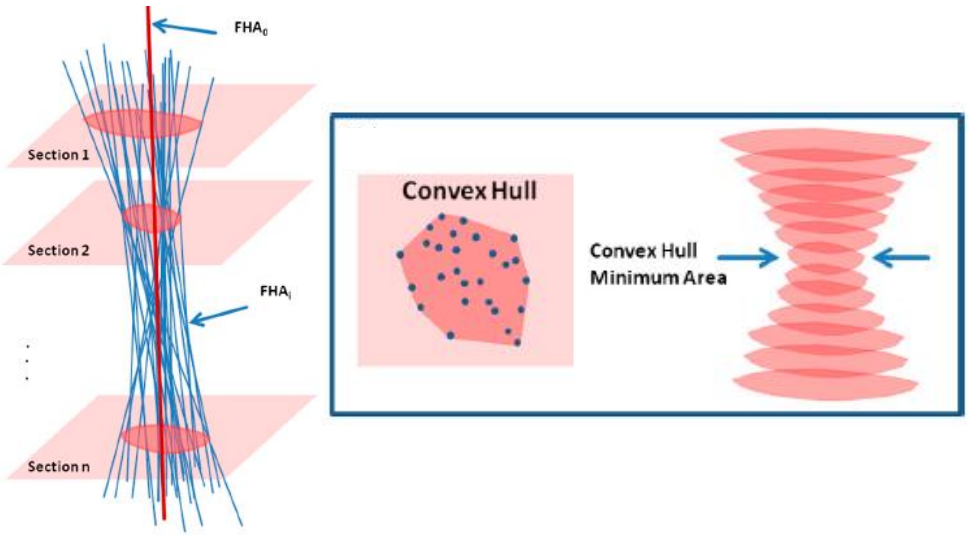

Figure 2-3: HAs during head rotation. For each plane perpendicular to FHA_0, convex hull of the intersections is computed, and minimum convex hull area is used as parameter to quantify HA behavior. Image adapted from [6]

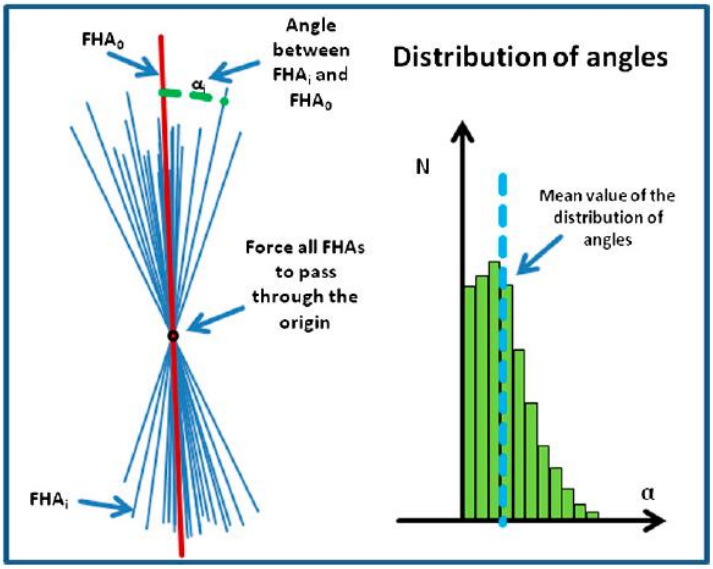

Figure 2-4: distribution of angles between HA_0 and each HA_i. Image adapted from [6]

Barbero et al [29] studied the reliability of HA parameters intra- and inter-session during planar cervical movement. Results depended on the type of movement. The intra- and inter-session reliability of convex hull area (CHA) and mean angle (MA) were "almost perfect" during rotation whereas CHA was "substantial" during lateral bending and MA ranged from "fair" to "substantial" during flexion-extension and lateral bending. These results confirmed the reliability of HA parameters to evaluate neck function.

A more recent study by the same authors introduces a new HA parameter to quantify humeral kinematics [27]. The barycenter of the intersection points was used as reference to compute the distance to each point and the mean distance (MD) to the barycenter was calculated for each plane. The output measurement is the minimum value (MMD = minimum mean distance) from the series of MD computed for each plane (Figure 2-5). MMD, together with mean angle (MA) mentioned above, were estimated for all volunteers in order to compare dominant to non-dominant side. Results demonstrated a significantly lower MA value on the dominant side and MMD was also lower for the dominant side, which means less dispersion of the axis.

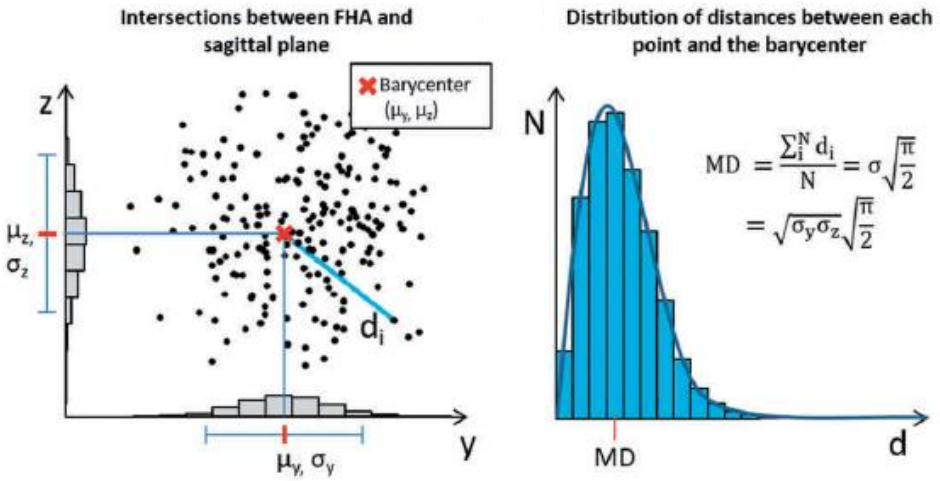

Figure 2-5: Intersections between FHAs and sagittal plane (left) and distribution of distance between each intersection point and the barycenter (right). Image adapted from [27]

Alsultan et al. [30] studied HA parameters during active neck movements at different speed (natural, slow and fast) in subjects with and without chronic neck pain (CNP). Results show less variability in CNP patients. Furthermore, higher MA variability was seen at the faster speed than slower for both subject groups, which shows the importance of movement speed since patients with CNP find difficulties performing rapid movement of their head.

Arin et al. [28] designed a methodology to identify aberrant neck kinematics and assess it. A neck circumduction is analyzed with the instantaneous helical axis approach in non-specific neck pain and in symptom-free subjects. The azimuthal angle was defined for each IHA tip. Aberrant motion was defined where the numerical derivative of this angle was negative, indicating where the IHA folds back upon itself (Figure 2-6). The number of "folds" exhibited within the asymptomatic group was 0.63 while symptomatic group was 4.00 and it decreased to 3.15 for subjects following treatment.

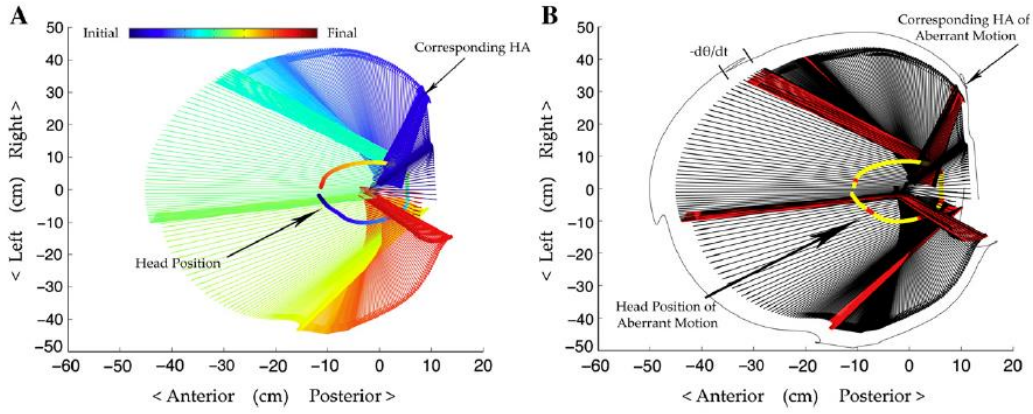

Figure 2-6: IHA and corresponding head position during neck circumduction of symptomatic subject. Folds were detected where numerical derivative of azimuthal angle was negative. Image adapted from [28]

2.1. FHA calculation methods

Every rotation of an object in space is defined by its axis and the amount of rotation around it. Given the initial and final position and orientation of the object, the axis vector and its position are calculated. To determine these variables, it is required to know the coordinates of at least three non-collinear points of the rigid body. It is also possible to obtain the characteristics of the axis knowing the initial and final position of one point and its rotation matrix. There are several methods to calculate finite displacement, they differ in the input variables and the algorithm used to process them.

Vectorial algebra method

This method used the Rodrigues displacement equation [32] to calculate the finite helical axis. The Rodrigues vector Ω formula (2) depicts a rotation of a vector in space given the axis and the angle of rotation. It has the same direction as the rotation axis u, and its value is the tangent of half the rotation angle θ:

$$\Omega = \mathrm{tg}\left(\frac{\theta}{2}\right) \cdot u \tag{2}$$

The equation of this method for Rodrigues displacement (3) requires the initial i and final position j variables of three points p, q, r and it relates the rigid-body displacements to the spatial coordinates of such points. The other parameters involved in the FHA calculation are the axis translation magnitude s and the axis point v. By clearing FHA displacement equations (3), the Rodrigues vector Ω is calculated (4). Normalizing this vector, the axis unit vector $u = \frac{\Omega}{\|\Omega\|}$ is obtained; therefore, is it also possible to calculate the angle of rotation by clearing equation (2). Furthermore, it is also possible to obtain a point in the axis (5) and the axis translation magnitude (6).

$$\left.\begin{aligned} p_j - p_i &= \tan\left(\frac{\phi}{2}\right) \cdot u \times \left(p_j + p_i - 2v\right) + su \\ q_j - q_i &= \tan\left(\frac{\phi}{2}\right) \cdot u \times \left(q_j + q_i - 2v\right) + su \\ r_j - p_i &= \tan\left(\frac{\phi}{2}\right) \cdot u \times \left(r_j + r_i - 2v\right) + su \end{aligned}\right\} \tag{3}$$

$$\Omega = \frac{\left[\left(q_j - q_i\right) - \left(r_j - r_i\right)\right] \times \left[\left(p_j - p_i\right) - \left(r_j - r_i\right)\right]}{\left[\left(q_j - q_i\right) - \left(r_j - r_i\right)\right] \cdot \left[\left(p_j + p_i\right) - \left(r_j + r_i\right)\right]} \tag{4}$$

$$v = \frac{1}{2}\left[\frac{u \times (p_j - p_i)}{\tan\left(\frac{\phi}{2}\right)} - [u \cdot (p_j + p_i)]u + p_i + p_j\right] \quad (5)$$

$$s = u \cdot (p_j - p_i) = u \cdot (q_j - q_i) = u \cdot (r_j - r_i) \quad (6)$$

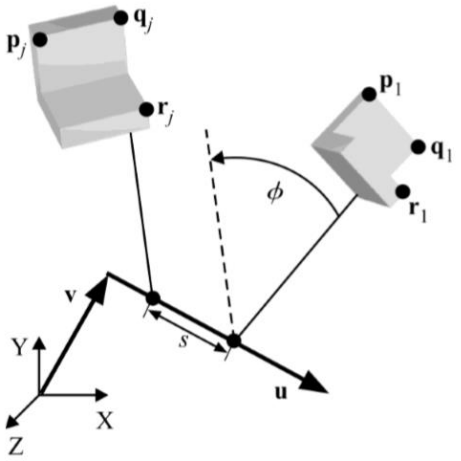

Figure 2-7: FHA and rigid body displacement parameters. Image adapted from [32]

Virtual body method

This method designed by Page et al. [33] also utilises the calculation of the Rodrigues vector but instead of manipulating vectors as the previous method, it uses an intermediate body whose points are the midpoints of each pair of homologous points at the initial and final position. On this virtual body, a field of half-displacements can be defined. A rigid body with a set of P_i markers $(i \geq 3)$ is assumed. The vector from the centroid of the markers G to each point P_i is denoted by r_i. After the displacement, the body is rotated an angle θ and the variables H, P_i, r_i, G change to H', P_i', r_i', G' (Figure 2-8.A).

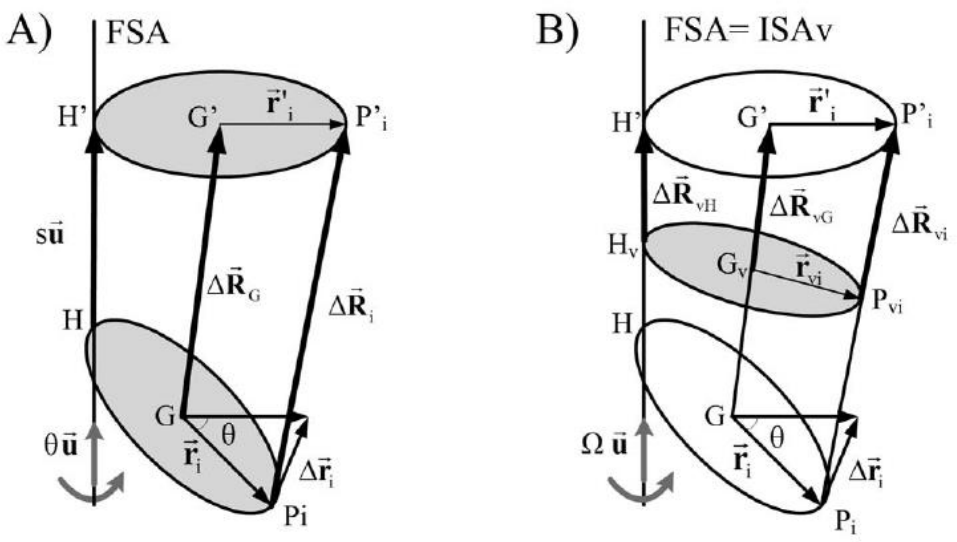

Figure 2-8: A) Finite displacement. B) Virtual displacement defined on the virtual body. Image adapted from [33]

In order to approach this problem, virtual body points P_{v_i} are defined as the midpoint between the initial P_i and final position P_i' (Figure 2-8.B) from equation (7). The centroid of the virtual body G_v is also calculated from the initial and final position of the centroid (8):

$$(P_i, P_i') \rightarrow P_{v_i}, \qquad OP_{v_i} = R_{v_i} = \frac{R_i' + R_i}{2} \tag{7}$$

$$OG_{v_i} = \frac{OG' + OG}{2} = R_{G_v} = \frac{1}{n}\sum R_{v_i} \tag{8}$$

The position of the vector for each virtual point P_{v_i} measured from the virtual centroid G_v is denoted by r_{v_i} (9):

$$r_{v_i} = \frac{r_i' + r_i}{2} = R_{v_i} - R_{G_v} \tag{9}$$

Finally, the vector field of virtual displacements ΔR_{v_i} and Δr_{v_i} are defined by equation (10) and (11) respectively.

$$\Delta R_{v_i} = \frac{1}{2}\Delta R_i = \frac{R_i' - R_i}{2} \tag{10}$$

$$\Delta r_{v_i} = \frac{1}{2}\Delta r_i = \frac{r_i{}' - r_i}{2} \tag{11}$$

This vector field corresponds to a skew-symmetric field so Rodrigues' formula can be rewritten by equation (12):

$$\frac{r_i{}' - r_i}{2} = \tan\left(\frac{\theta}{2}\right) u \times \frac{r_i' + r_i}{2} \tag{12}$$

And replacing by the terms calculated above (9), that equation is finally defined by (13):

$$\Delta R_{v_i} = \Delta R_{v_G} + \Omega \times r_{v_i} \tag{13}$$

Where omega is the Rodrigues vector, parallel to the FHA and whose relationship with the rotation angle is defined by equation (2), which can be rewritten as (14):

$$\Omega = \tan\left(\frac{\theta}{2}\right) u = \bar{J}_{v_G}^{-1} \sum r_{v_i} \times \Delta R_{v_i} \tag{14}$$

Being $\bar{J_G}$ the inertia tensor of the virtual points given by equation (15):

$$\bar{J}_G = \begin{bmatrix} \sum (y_i^2 + z_i^2) & -\sum x_i y_i & -\sum x_i z_i \\ -\sum x_i y_i & \sum (x_i^2 + z_i^2) & -\sum y_i z_i \\ -\sum x_i z_i & -\sum y_i z_i & \sum (x_i^2 + y_i^2) \end{bmatrix} \tag{15}$$

Normalizing Ω, axis unit vector $u = \frac{\Omega}{\|\Omega\|}$ is obtained; therefore, it is also possible to calculate the angle of rotation by clearing equation (2). The field of virtual displacement (12) has the same structure as the velocity field so that the distance between the virtual centroid G_v and a point in the axis H_v can be expressed by equation (16):

$$G_v H_v = \frac{\Omega \times \Delta R_{v_G}}{\Omega^2} \tag{16}$$

Geometric algebra method

This method proposed by Beggs [35] estimates the HA from three points of the rigid body by performing geometric manipulations on the vectors formed by the points before and after the displacement. The three vectors connect points position before and after displacement: $P_i P_i'$ $(i = 1, 2, 3)$. Those vectors are moved parallel to themselves until the

points P_1, P_2, P_3 (points before displacement) coincide with the origin of the global reference. In this configuration, P_1', P_2', P_3' (points after displacement) form a plane which is perpendicular to the HA and is located at a distance s from the origin. That plane is defined by equation (17), being $(e_x\ ,\ e_y\ , e_z)$ the unit vector of the axis u perpendicular to the plane formed by P_i' points.

$$e_x x + e_y y + e_z z = s \tag{17}$$

The vectors $P_i P_i'$ have the coordinates $[\Delta_i x \quad \Delta_i y \quad \Delta_i z]$, where $\Delta_i x = x_i' - x_i\ ;\ \Delta_i y = y_i' - y_i\ ;\ \Delta_i z = z_i' - z_i$. The ends of these vectors belong to the normal plane to the FHA, therefore equation (17) can be written after some manipulations in matrix form for all these points (18):

$$\begin{bmatrix} e_x/s \\ e_y/s \\ e_z/s \end{bmatrix} = \begin{bmatrix} \Delta_1 x & \Delta_1 y & \Delta_1 z \\ \Delta_2 x & \Delta_2 y & \Delta_2 z \\ \Delta_3 x & \Delta_3 y & \Delta_3 z \end{bmatrix}^{-1} \cdot \begin{bmatrix} 1 \\ 1 \\ 1 \end{bmatrix} = K \tag{18}$$

Knowing that e is a unit vector, whose norm is equal to 1, s can be extracted from equation (18) and therefore it is also possible to calculate e. By defining a vector v_1 from point P_1 to point P_2, the vector $v_1 \times e$ is rotated by an angle θ when the rigid body rotates by the same amount around the FHA. After rotation, vector v_1 is transformed into vector v_2, connecting point P_1' to point P_2' . Therefore, the angle of rotation can be calculated as the angle between v_1 and v_2 (19):

$$\cos(\theta) = \frac{v_{(1)} \times e}{\left\| v_{(1)} \times e \right\|} \cdot \frac{v_{(2)} \times e}{\left\| v_{(2)} \times e \right\|} \tag{19}$$

Rotation matrix method (displacement transformation matrix)

This method extracts the helical axis characteristics from the rotation matrix R of the rigid body and the position of one point [34]. It is based on the concept of invariance when changing the reference system. Having the initial P_0 and final P_1 position of a point, the rotation matrix ${}^1_0R$ allows us to orientate the final position P_1 relative to the initial position P_0. Equation (20) shows the relationship between those parameters.

$$P_0 = {}^1_0R \times P_1 \tag{20}$$

As u is the direction of the axis, $R \times u = u$, since the axis remains fixed in space. The solution of the equation is unique unless $R = I$. That equation may be rewritten as $R \cdot u = I \cdot u$ so that $(R - I) \cdot u = 0$, which means that u is an eigenvector of R corresponding to the eigenvalue $\lambda = 1$. Since u is a skew-symmetric matrix, it can be calculated by (21) and (22). Finally, equation (23) shows the relationship between R terms and rotation axis direction u.

$$[u]_x = (R - R^T) \tag{21}$$

$$(R - R^T) \cdot u = [u]_x \, u = u \times u \tag{22}$$

$$R = \begin{bmatrix} a & b & c \\ d & e & f \\ g & h & i \end{bmatrix} \rightarrow u = \begin{bmatrix} h - f \\ c - g \\ d - b \end{bmatrix} \tag{23}$$

Two methods are possible for the determination of the angle of rotation around the axis (24).

$$\theta = \begin{cases} \cos^{-1}\left(\dfrac{R_{11} + R_{22} + R_{33} - 1}{2}\right) \\ \sin^{-1}\left(\sqrt{u_{23}^2 + u_{31}^2 + u_{12}^2}\right) \end{cases} \tag{24}$$

Single value decomposition method

This method applies the singular value decomposition algorithm (SVD) to calculate the rotation matrix from the initial and final position of a series of N points [36]. The SVD algorithm consists of decomposing a matrix into a product of three matrices. The initial positions of the points are defined by $m_1, m_2, \ldots, m_n$ while the final positions are $r_1, r_2, \ldots, r_n$ (Figure 2-9).

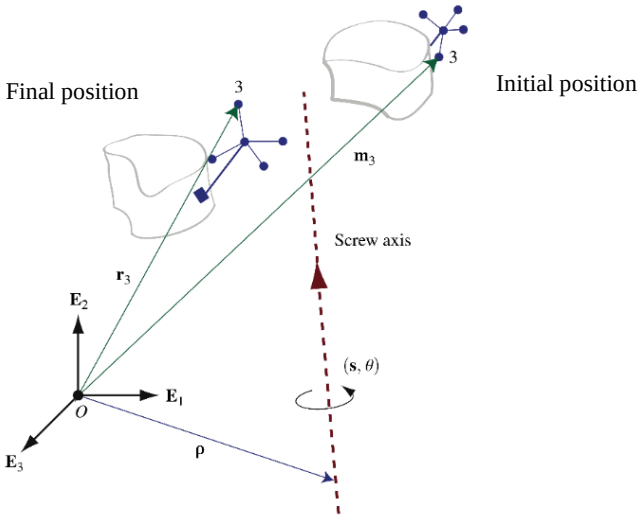

Figure 2-9: Positions of the rigid body before m_i and after r_i rotates an angle theta

The first step for applying the SVD method involves computing the centroid of the set of points before (25) and after (26) the displacement:

$$\bar{m} = \frac{1}{4} \cdot (m_1 + m_2 + m_3 + m_4) \tag{25}$$

$$\bar{r} = \frac{1}{4} \cdot (r_1 + r_2 + r_3 + r_4) \tag{26}$$

The next step involves constructing a matrix S from the distance of each point of the rigid body relative to the centroid: $S = C \cdot D^T$, being C and D defined by equations (27) and (28):

$$C = \begin{bmatrix} (m_1 - \bar{m})\,\vec{i} & (m_2 - \bar{m})\,\vec{i} & (m_3 - \bar{m})\,\vec{i} & (m_4 - \bar{m})\,\vec{i} \\ (m_1 - \bar{m})\,\vec{j} & (m_2 - \bar{m})\,\vec{j} & (m_3 - \bar{m})\,\vec{j} & (m_4 - \bar{m})\,\vec{j} \\ (m_1 - \bar{m})\,\vec{k} & (m_2 - \bar{m})\,\vec{k} & (m_3 - \bar{m})\,\vec{k} & (m_4 - \bar{m})\,\vec{k} \end{bmatrix} \tag{27}$$

$$D = \begin{bmatrix} (r_1 - \bar{r})\,\vec{i} & (r_2 - \bar{r})\,\vec{i} & (r_3 - \bar{r})\,\vec{i} & (r_4 - \bar{r})\,\vec{i} \\ (r_1 - \bar{r})\,\vec{j} & (r_2 - \bar{r})\,\vec{j} & (r_3 - \bar{r})\,\vec{j} & (r_4 - \bar{r})\,\vec{j} \\ (r_1 - \bar{r})\,\vec{k} & (r_2 - \bar{r})\,\vec{k} & (r_3 - \bar{r})\,\vec{k} & (r_4 - \bar{r})\,\vec{k} \end{bmatrix} \tag{28}$$

Once the value of the matrix S is computed, the singular value decomposition algorithm is applied to it (29). As a result, three matrices $R_1,\ \wedge,\ R_2$ are obtained:

$$S = R_1 \wedge R_2 \tag{29}$$

R_1 and R_2 are orthogonal matrices and $\wedge$ is a diagonal matrix. Finally, the rotation matrix for the specific displacement is given by (30):

$$R^* = R_1 \cdot \begin{bmatrix} 1 & 0 & 0 \\ 0 & 1 & 0 \\ 0 & 0 & |R_1 \cdot R_2| \end{bmatrix} \cdot R_2 \tag{30}$$

The rotation matrix is calculated from the coordinates of the points before and after displacement, the FHA parameters are obtained following the same method as [34] which is summarized in the section *"Rotation matrix method"* of the present document by equations (23) and (24).

Unit quaternion method

This method developed by Horn [37] is based on the representation of the rotation by means of a unit quaternion. A quaternion can be defined as a vector with four components

$q = q_0 + q_x\vec{\imath} + q_y\vec{j} + q_z\vec{k}$, a composite of a scalar and an ordinary vector or a complex number with three different imaginary parts. The resolution requires the calculation of the eigenvector associated with the most positive eigenvalue of a symmetrical 4 × 4 matrix, whose elements are a combination of sums and products of coordinates of the different points in the rigid body before and after displacement. Once the unit quaternion is calculated, the rotation matrix can be determined. Analyzing the equation that relates the rotation matrix with the points before $p_{(1)_i}$ and after $p_{(2)_i}$ displacement (31), the term ε_i quantifies the error in rotation matrix calculation.

$$p_{(2)_i} = R \cdot p_{(1)_i} + d + \varepsilon_i \tag{31}$$

The accuracy in the calculation of this matrix will consist of minimizing the value of this error and maximizing the value of the remaining terms in equation (31). Being (32) the equation for that minimized value.

$$min\left(\frac{1}{m}\sum_{i=1}^{m}\|\varepsilon_i\|^2\right) \tag{32}$$

The algorithm begins by computing the centroids of the set of points before $\bar{p}_{(1)}$ and after $\bar{p}_{(2)}$, and the coordinates of the points relative to their centroid are obtained (33).

$$\begin{aligned} p'_{(1)_i} &= p_{(1)_i} - \bar{p}_{(1)} \\ p'_{(2)_i} &= p_{(2)_i} - \bar{p}_{(2)} \end{aligned} \tag{33}$$

Equation (32) is rewriting in terms of $p'_{(1)_i}$ and $p'_{(2)_i}$, resulting in equation (34):

$$max\left[\frac{1}{m}\sum_{i=1}^{m}\left({p'_{(2)_i}}^{T} \cdot R \cdot p'_{(1)_i}\right)\right] \tag{34}$$

Representing the rotation by means of a unit quaternion and after a few algebraic manipulations, the equation (34) can be rewritten as equation (35).

$$max(q^T \cdot N \cdot q) \tag{35}$$

Where q is the unit quaternion and N is a 4×4 symmetric matrix defined by equation (36). M_{ij} represents the elements of the matrix defined by $M = m \cdot C$, with m the number of points and C the correlation matrix whose coordinates are sums of products of coordinates before $p'_{(1)_i}$ and after $p'_{(2)_i}$ displacement (37).

$$N = \begin{bmatrix} (M_{11} + M_{22} + M_{33}) & M_{23} - M_{32} & M_{31} - M_{13} & M_{12} - M_{21} \\ M_{23} - M_{32} & (M_{11} - M_{22} - M_{33}) & M_{12} + M_{21} & M_{31} + M_{13} \\ M_{31} - M_{13} & M_{12} + M_{21} & (-M_{11} + M_{22} - M_{33}) & M_{23} + M_{32} \\ M_{12} - M_{21} & M_{31} + M_{13} & M_{23} + M_{32} & (-M_{11} - M_{22} + M_{33}) \end{bmatrix} \quad (36)$$

$$C = \frac{1}{m}\sum_{i=1}^{m} p'_{(2)_i} \cdot {p'_{(1)_i}}^T \quad (37)$$

The author demonstrated in [37] that the solution of the maximization in equation (35) is the eigenvector v of the matrix N corresponding to the most positive eigenvalue λ of the matrix:

$$|N - \lambda \cdot I| = 0 \quad (38)$$

$$N \cdot v = \lambda \cdot v \quad (39)$$

Once the unit quaternion q is estimated from equation (35) knowing the solution of the maximization by equation (38) and (39), the rotation matrix of the displacement is calculated by equation (40).

$$R = \begin{bmatrix} (q_0^2 + q_x^2 - q_y^2 - q_z^2) & 2(q_x q_y - q_0 q_z) & 2(q_x q_z + q_0 q_y) \\ 2(q_y q_x + q_0 q_z) & (q_0^2 - q_x^2 + q_y^2 - q_z^2) & 2(q_y q_z - q_0 q_x) \\ 2(q_z q_x - q_0 q_y) & 2(q_z q_y + q_0 q_z) & (q_0^2 - q_x^2 - q_y^2 + q_z^2) \end{bmatrix} \quad (40)$$

Finally, the FHA parameters are calculated following the same method as [34] which is summarized in the section *"Rotation matrix method"* by equations (23) and (24).

2.2. Thesis objectives

Six degrees of freedom approach is the most common method in human analysis due to the ease of interpretation by clinicians. However, it strongly depends on the chosen reference system, which introduces problems in the reliability of the results while comparing between patients. FHA approach solves this problem dependence since the parameters that describe its variability do not depends on the position and orientation in space relative to the chosen reference. Nevertheless, FHA struggles with problems related with calculation error and poor visualization techniques. This calculation error is inversely proportional to the angle step between the position before and after displacement. The main objective of this thesis is to compare different FHA calculation methods in order to look for the minimization of error sensitivity. The optimal FHA calculation algorithm will be decided on the least error method for cervical movement analysis and it will be implemented in a user-friendly software to analysis patient cervical motion through parameters that depict the behavior of all FHAs for the entire movement.

Chapter 3

3. Materials and methods

3.1. Data acquisition

Cervical spine movements (flexion-extension, rotation and lateral bending) were recorded using Polhemus, an electromagnetic tracking system which delivers true 6 degrees of freedom: it measures not only position but also the orientation of the sensor. The object position is tracked within x, y, z coordinates as well as the object's orientation (yaw, pitch and roll). The tracking system used is called Polhemus LIBERTY and it supports four sensors, each operating at up to 240 Hz. The sensor (Figure 3-1) measures the low-frequency magnetic field generated by the source and it is used to track both the position and orientation of the object to which it is attached, relative to the measurement reference frame, called cube reference or source (Figure 3-2). It has a static accuracy of 0.03 in. (0.7620 mm) RMS for X, Y or Z position and 0.15° RMS for sensor orientation. The source generates the low-frequency magnetic field measured by the sensor. The source's X, Y, and Z-axes are the default measurement reference frame [38]. Those components are connected to the rear of the central module (Figure 3-3).

Figure 3-1: Electromagnetic sensor. Image adapted from [38].

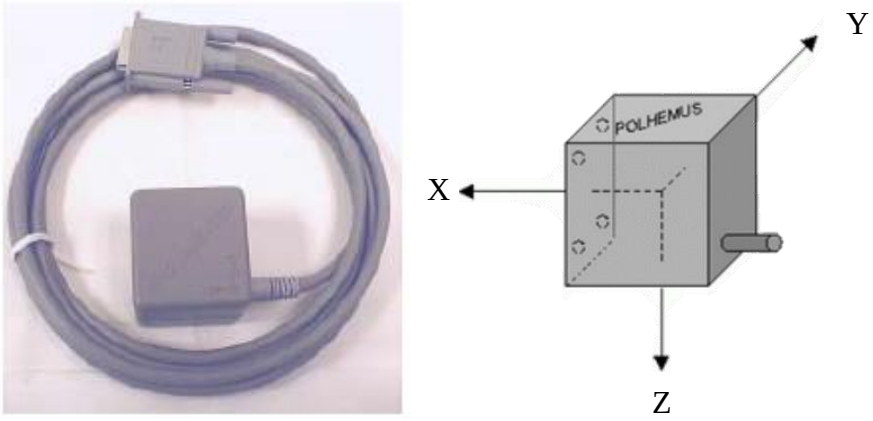

Figure 3-2: Source/cube reference. The reference frame of the tracking system. Image adapted from [38].

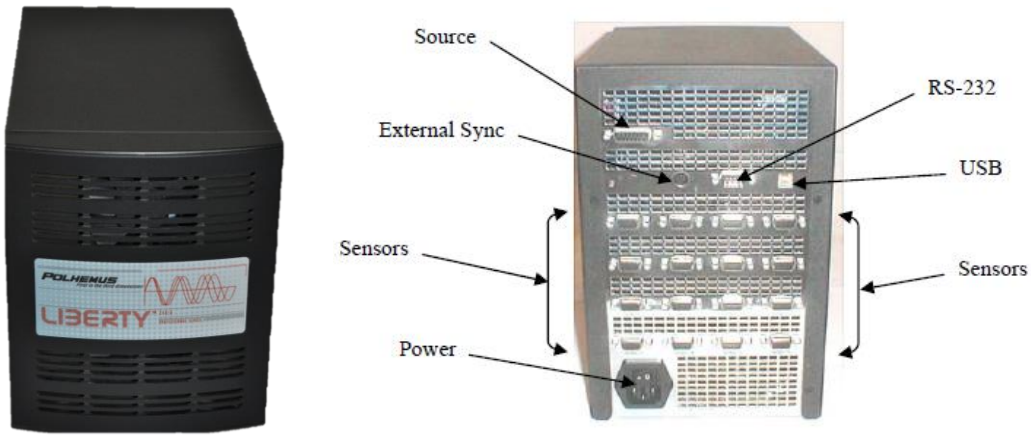

Figure 3-3: front (left) and rear (right) of the central module. Image adapted from [38].

The data was collected by physiotherapy students from "Vrije Universiteit Brussel" and a standard protocol was followed by all the student-investigators to collect the data for each head movement. Three sensors are used for the data registration. One measures head movement, another small displacement of the thorax during head movement and the last verifies whether there is disturbance during the movement registration. Protocol steps are explained below:

1. Subjects were instructed to sit on the chair and to look straight ahead with their arms on their thighs.
2. Sensor 1 is fixed to a headband placed around the forehead.
3. Sensor 2 was fixed to a band placed on the breastbone/sternum.
4. Sensor 3 and the cube reference (source) are positioned on a wooden table. The cube reference is positioned in such a way that the orientation of its x, y, z axes coincides with the actual rotatory axes for the three types of cervical movement (flexion-extension, axial rotation and lateral bending).
5. The movement is performed twice prior to the registration, which served as a training.

Figure 3-4: Conditions of the measurement protocol explained above.

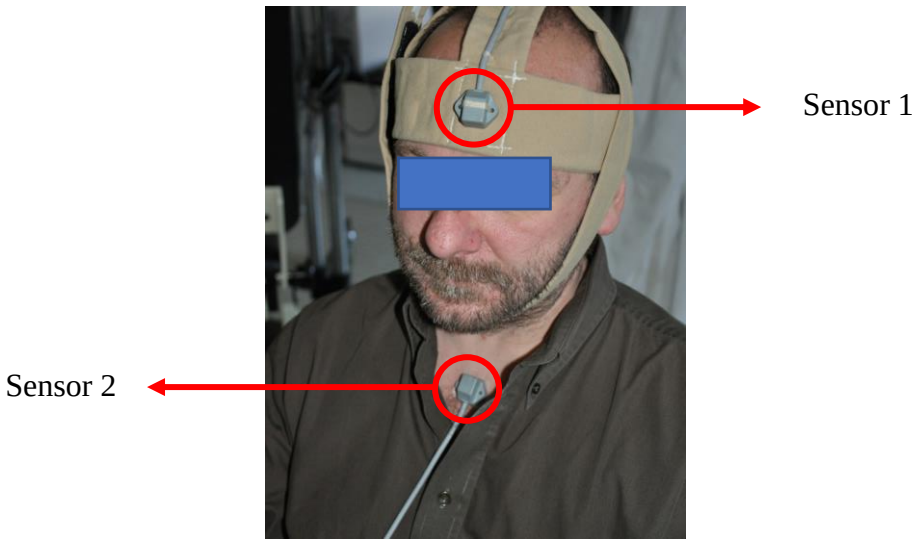

Figure 3-5: Location of sensors 1 and 2 (measurement protocol).

Figure 3-6: Movement performance (head rotation)

Once the movement is performed, the data is exported via the Polhemus software. This interface allows the user to export different variables that characterize the movement, from which the following are selected for all records:

- Coordinates x, y and z of the three sensors relative to the cube reference.
- Direction cosines of each sensor: the cosines of the angles between the sensor's x, y, z axes and the X, Y, Z axes of the measurement reference frame (see Figure 3-2).
- Distortion level: '0', '1' or '2'. It measures the interferences during the registration caused by high light levels, high sound levels, or high metallic distortion. If this value is not equal to 0 the data cannot be taken as valid.

This data is arranged as a matrix where the columns correspond to the variables mentioned above and the rows to the corresponding sensors, being each set of three consecutive rows (sensor 1, 2 and 3) part of the same frame (time instant). Consequently, the dimension of the data matrix is 14 × (nº of frames × 3):

		coordinates x, y, z			direction cosines x axis			y axis			z axis			dist. level
1st frame	1	22,78	40,65	-21,10	-0,21	0,96	0,12	-0,23	-0,17	0,95	0,94	0,17	0,26	0
	2	22,44	40,87	-10,02	0,47	-0,80	-0,36	0,76	0,16	0,62	-0,44	-0,57	0,69	0
	3	17,36	40,53	-11,44	0,08	0,69	-0,71	-0,89	0,36	0,24	0,43	0,62	0,65	0
2nd frame	1	22,78	40,65	-21,10	-0,21	0,96	0,12	-0,23	-0,17	0,95	0,94	0,17	0,26	0
	2	22,44	40,87	-10,02	0,47	-0,80	-0,36	0,76	0,16	0,62	-0,44	-0,57	0,69	0
	3	17,36	40,53	-11,44	0,08	0,69	-0,71	-0,89	0,36	0,24	0,43	0,62	0,65	0
	…	…	…	…	…	…	…	…	…	…	…	…	…	…

Figure 3-7: Arrangement of data in matrix form.

Variables of sensor 3, both positions and orientations, must remain constant throughout the entire movement in order to qualify the data registration as valid. This is because the cube reference is located on the same surface as sensor 3, so changes in coordinates of that sensor during movement would mean that the reference frame had also moved. Therefore, the coordinates and positions of the sensors located on the forehead and sternum would vary and be erroneous. This method together with the distortion level number named above is used to validate the data registration.

3.2. Kinematic analysis

This section explains the detailed process for kinematic parameters calculation, which are used to describe human movement. All motion analysis was performed in MATLAB, a multi-paradigm numerical computing environment and proprietary programming language developed by MathWorks. It allows matrix manipulations, plotting of functions and data, implementation of algorithms or creation of user interfaces.

Change in reference system

Sensor 2 is located on the breastbone as described in Figure 3-5. Cervical spine movements imply small movements of shoulders and thorax. That is why the coordinates of sensor 2 are not constant during cervical movement (Figure 3-8). Those small variations also impact on sensor 1 coordinates, which is the one located in head.

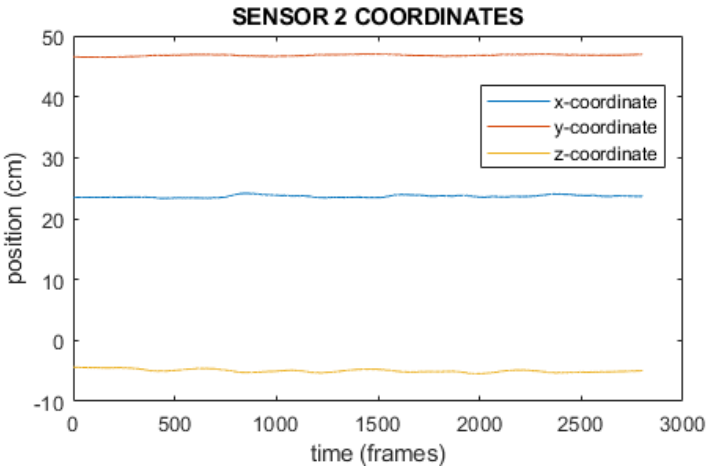

Figure 3-8 : Coordinates during motion of sensor 2 (located on the breastbone) relative to cube reference.

The aim of this study is to analyze cervical spine movement. Therefore, head movement relative to the thorax must be calculated. In order to achieve this, it is required to change the reference system (change of basis) of the sensor 1 position. From now on, the (0, 0, 0) point is located on the breastbone (sensor 2). This change of basis is defined by equation (41):

$$P_A(i) = {}^A_B R(i) \cdot P_B(i) + {}^A_B O(i)\ ;\ i = nº\ frames \qquad (41)$$

Where P_A is the coordinates of sensor 1 expressed in the cube reference (known), ${}^A_B R$ is the rotation matrix that defines the orientation of the new reference system and ${}^A_B O$ are the coordinates of sensor 2 expressed in cube reference (known). As the new reference system has the same orientation as the cube reference, the rotation matrix for this case is the identity matrix. Clearing P_B term, the head position relative to the thorax is obtained for the entire movement.

Rigid body 3-D motion parameters

As detailed in section 2.1. FHA calculation methods of state-of-the-art chapter, there are some FHA calculation algorithms that operate with the position of three non-colinear points of the rigid body and others that work with the position of one point and its displacement transformation matrix. Both ways were implemented in order to estimate FHA using the six methods described in 2.1. section.

For that dataset, only the coordinates of one sensor (sensor 1) are known but also the orientation (direction cosines) of its x, y, z axes. Therefore, it is possible to estimate the position of three more points belonging to the head from the orientation matrix, which is defined by unit vectors of x, y and z axes of sensor 1 (Figure 3-9).

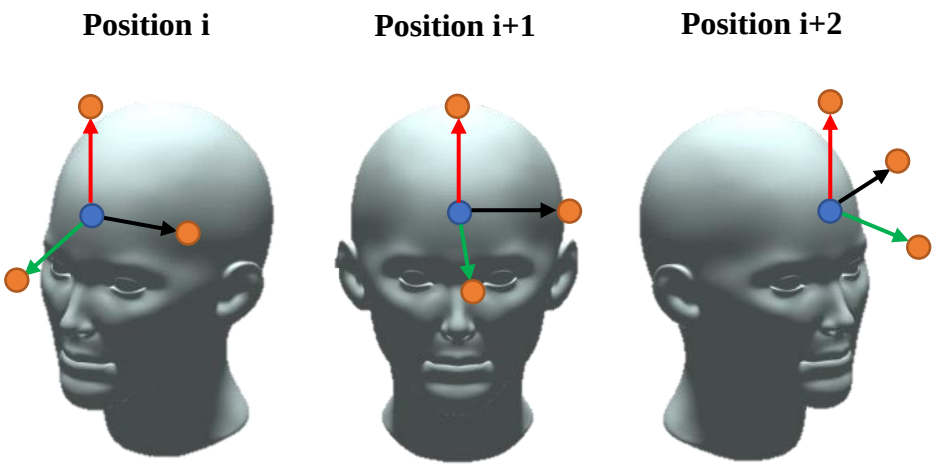

Figure 3-9: Estimation of three more points (orange points) of the rigid body from the direction cosines of sensor 1 (blue point). The green, red and black axis correspond to the x, y and z axis of sensor 1.

The displacement transformation matrix is also estimated from the direction cosines of sensor 1. The transformation matrix depicts the displacement from position i to position $i+1$. This matrix is defined by the projection of position $i+1$ axes in position i axes (42) and it is represented in Figure 3-10.

$$RM = \begin{bmatrix} A(x) & B(x) & C(x) \\ A(y) & B(y) & C(y) \\ A(z) & B(z) & C(z) \end{bmatrix} \quad (42)$$

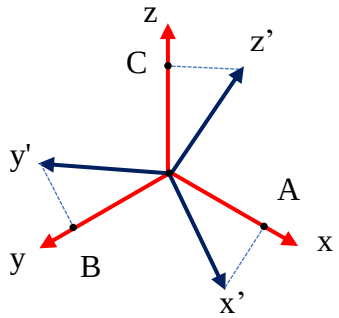

Figure 3-10: Projections (A, B, C) of position i+1 axes (x', y', z') in position i axes (x, y, z)

For the calculation of this transformation matrix, a new change of basis is used (43). In this case, P_A and P_B are the orientation matrix in space of position $i+1$ and i relative to the reference and the rotation matrix R is the projection of position $i+1$ axes in position i axes (displacement transformation matrix).

Position smoothing

Movement of the head corresponds to a continuous function that is measured with motion tracking systems as discrete data due to the sampling frequency, which is 240 Hz for the Polhemus LIBERTY electromagnetic tracking system. Furthermore, measured data have errors due to the accuracy of the tracker which is 0.00015 in. (0.038 mm) at 12 in. (30 cm) for position and 0.0012° for orientation with that technology [38].

Therefore, it is necessary to "reconstruct" functions from the observation of discrete series. The reconstructed function must be error-free, continuous and differentiable. Adjustment of functions is a preliminary step in motion analysis to calculate derivates since errors are accentuated when deriving.

Smoothing using B-splines (basic soft polynomial line) was used for positions. A spline is a function defined piecewise by polynomials at intervals given by a series of points, called nodes (knots). The order of the polynomials was set to 5 in order to obtain a smooth second derivative [39] and the number of nodes to 100 (the greater the number of nodes, the better the approach). The resulting function is therefore a combination of different polynomials (43) where $\phi_k(t)$ is the kth basis function [40].

$$f(t) = a_1\phi_1(t) + a_2\phi_2(t) + \cdots + a_k\phi_k(t) \tag{43}$$

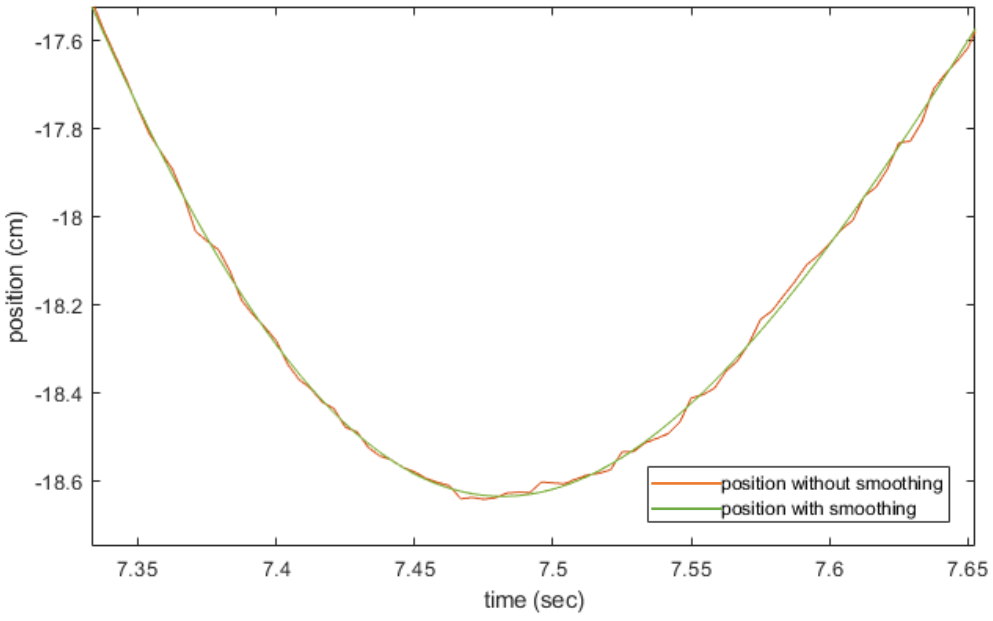

Figure 3-11 : Result of applying B-splines smoothing to data. Orange curve is the positions of the sensor without smoothing and green one after applying smoothing.

Once the adjustment function for position is obtained, it is possible to obtain linear velocity and linear acceleration by means of the first and second derivative.

Angular velocity

The relation between angles and angular velocity is not as evident as the relation between displacement vector and linear velocity. The problem arises from the fact that finite rotations are not composed as a sum (while angular velocities are, because they are infinitesimal rotations). Not even the composition of a finite displacement and an infinitesimal one is composed as a sum. In other words, a finite rotation is not defined as a vector, even if it is represented as such. This problem is reported by [33] and it is explained in Figure 3-12.

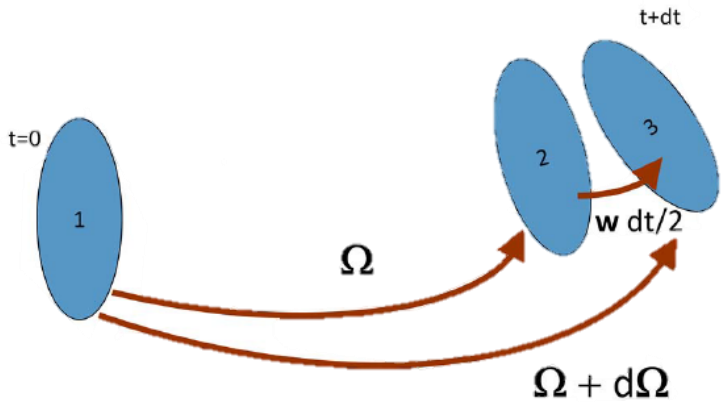

Figure 3-12: Composition of a finite rotation Ω and the infinitesimal angle displacement $d\phi = w\,dt\,/\,2$.

At the initial instant the solid is in the reference position, 1. At the end of a time t, it has undergone a finite displacement given by the rotation that is represented by means of Ω (Rodrigues vector) and it is in position 2. After a time dt, the object has moved from position 2 to position 3 an infinitesimal displacement whose rotation is $w \cdot dt\,/\,2$. The displacement from position 1 to 3 is equal to $\Omega + d\Omega$, and is expressed by equation (44) which is formed by applying the general expression for composing rotations using Rodrigues vector:

$$\Omega + d\Omega = \frac{\Omega + (w\,dt/2) - (\Omega \times w\,dt/2)}{1 - (\Omega \cdot w\,dt/2)} \tag{44}$$

Finally, $w \cdot dt\,/\,2$ is estimated as a result of two displacements: the first one is performed from position 2 to 1 $(-\Omega)$ and the second one from position 1 to 3 $(\Omega + d\Omega)$:

$$\frac{w \cdot dt}{2} = (-\Omega) \oplus (\Omega + d\Omega) \approx \frac{d\Omega + \Omega \times (\Omega \times d\Omega)}{1 - \Omega^2} \tag{45}$$

From where the expression of w based on $d\Omega/dt$ is obtained:

$$w = \frac{2}{1+\Omega^2}\left(\frac{d\Omega}{dt} + \Omega \times \frac{d\Omega}{dt}\right) \quad (46)$$

This angular velocity calculation algorithm from Rodrigues vector is computationally more efficient than the calculation algorithm from linear velocities v_i and positions r_i of each point since that calculation, given by equation (47) would imply derivation of all points of the rigid body and calculation of the inertia tensor, which in a situation with a large number of points would be computationally expensive. Furthermore, Rodrigues vector is calculated during the kinematic analysis [39] because by means of it, the angular displacement for each position is estimated due to the relation between the Rodrigues vector value and the tangent of half the rotation angle (2). Furthermore, two FHA methods are based on the Rodrigues calculation, so its estimation is useful for many later calculations.

$$w = J_G^{-1} \Sigma r_i \times v_i \quad (47)$$

3.3. Angle steps of FHA estimations

FHA is the rotation axis around which the displacement of a body occurs. This displacement between two different positions is called angle step. The entire movement is divided into finite displacements given an angle step. For that, extreme and neutral positions of the movement are defined (Figure 3-13). Neutral positions coincide with the points where the angle is equal to zero, and extreme positions are calculated as the local maximum and minima of angles around the axis where the main rotation is performed. First and last extreme positions are not considered since they coincide with the beginning and the end of the movement and the patient may be conditioned to change the velocity.

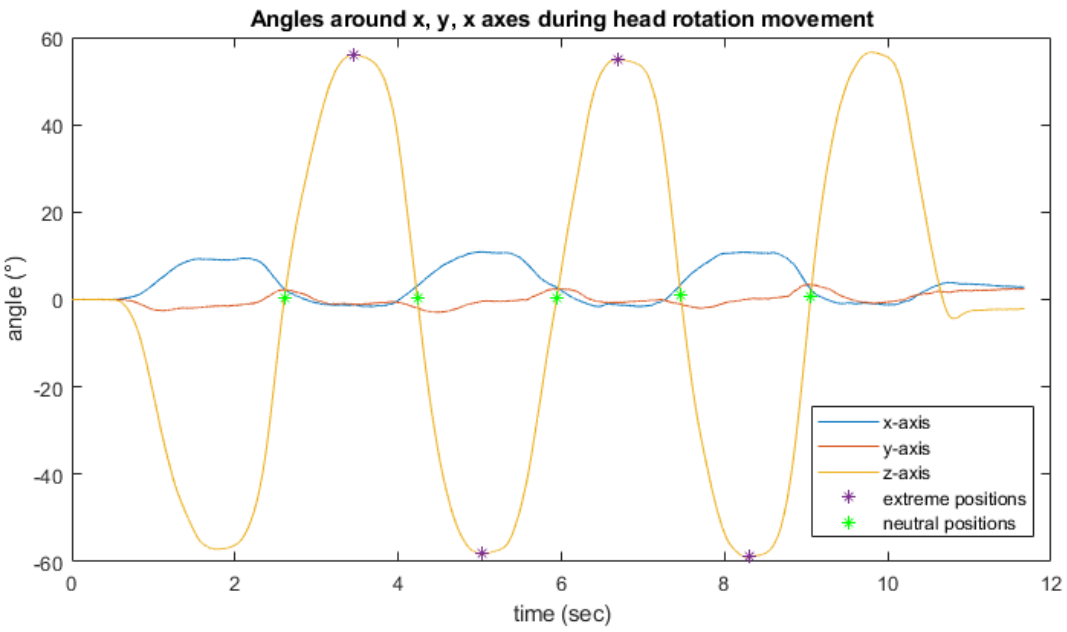

Figure 3-13: Head rotation movement around z-axis. Extreme and neutral positions of angles are defined

Extreme points may adopt two types of positions in head movements: left and right (for axial rotation and lateral bending) or flexion and extension (for flexion-extension). This fact defines the angle sign (positive or negative). The movement that occurs from i to $i + 1$ extreme position is defined as a cycle. As a result, a sample with n extreme points will have $n - 1$ cycles. Each cycle is equally divided in steps at a defined angle (Figure 3-14). FHA is calculated between each step. The set of FHAs for all cycles characterizes the entire movement and as a result, the movement is divided in finite displacements. The smaller the angle, the greater the number of FHAs that define the movement (Figure 3-15).

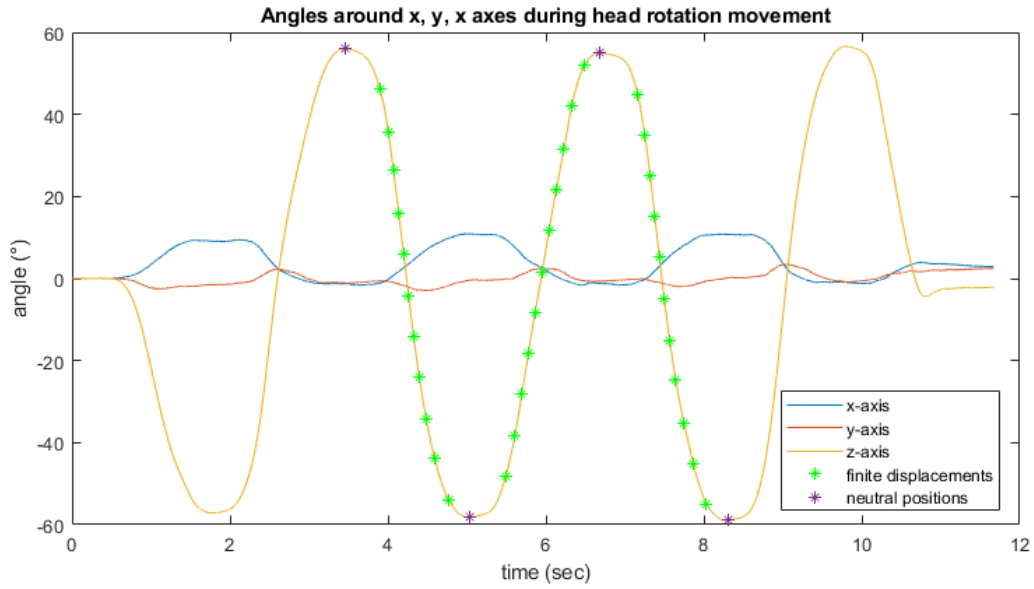

Figure 3-14: Head rotation movement where each cycle is equally divided into steps at a defined angle. For this sample, angle step was set to 10 degrees.

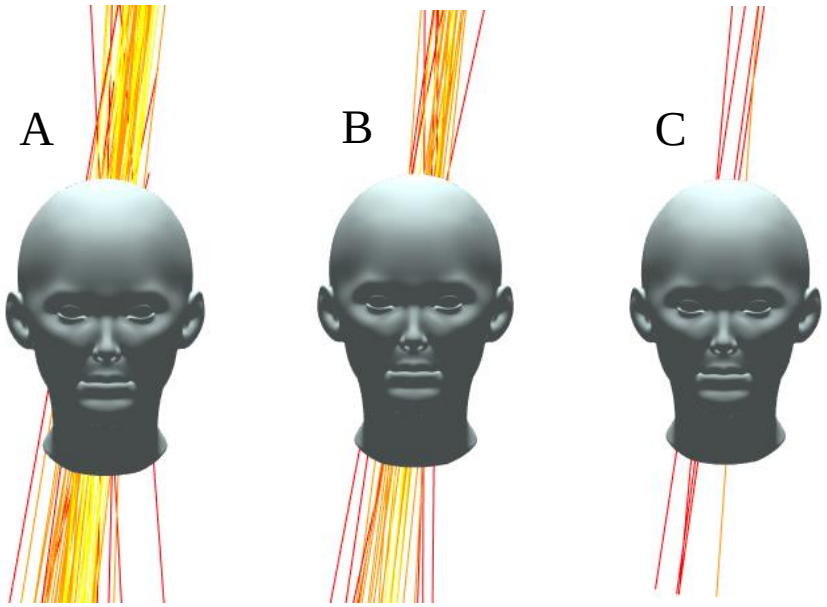

Figure 3-15 : Effect of step angle on FHAs for the same movement data. A: 5°, A: 10°, A: 30°.

3.4. Optimization of FHA estimations

As reported in "2.1. FHA calculation methods" there are several methods to calculate FHA based on different algorithms and techniques. Those methods are explained in state-of-the-art chapter and are listed below:

- Vector algebra method (method 1)
- Displacement transformation matrix method (method 2)
- Geometric algebra method (method 3)
- Virtual body method (method 4)
- Single value decomposition method (method 5)
- Unit quaternion method (method 6)

All methods were implemented in MATLAB through the equations that define them. For each method FHA parameters such as FHA axis direction u, angle of rotation around the axis θ, translation vector along the axis q, quantity of translation along the axis qt and a point in the axis p_0 were defined.

The objective in FHA optimization is to reduce error-prone in FHA estimation for cervical movements so that the most efficient calculation algorithm will be the one with the least error-prone. In order to achieve this, the estimated parameters are compared with the value of the true parameters. Absolute error is the difference in the measured (estimated by the algorithms) and the real values. Since the actual value of FHA parameters are not known for cervical movement registrations, two procedures were performed to evaluate the effectiveness of FHA algorithms. The first one is based on a rotating object test using Polhemus electromagnetic tracking system to record rotatory motion. The second procedure is a simulation of body movement performed in MATLAB by adding Gaussian noise to position and orientation of the points. Since the real axes in

these simulations can be calculated, it is possible to obtain FHA calculation error for each method.

Axis direction u is estimated by applying the specific equations of each algorithm. For axis position p_0, the same equation is used for the six methods (48). It consists in projecting the mid-point of the segment connecting the two centroids in the final p' and initial p positions of the rigid body on the axis. Quantity of translation around the axis qt is calculated by projecting the displacement vector between initial and final position onto the axis direction.

$$p_0 = \frac{1}{2}(p + p') + 2 \cdot \mathrm{tg}\left(\frac{\theta}{2}\right)^{-1} \cdot \left(u \times (p' - p)\right) \tag{48}$$

The rotating object test was used to decide the most effective algorithm since its movement was recorded using Polhemus tracking system, same as cervical movement data. After that, MATLAB motion simulation was used to evaluate the effect of introducing noise in position and orientation on FHA parameters (u, p_0, qt). The influence of different angle steps on those parameters was also evaluated. The design protocol of each procedure is explained in detail below.

3.4.1. Rotating object test

The test object is a PMMA disk (70 mm radius) to undergo rotatory motion. A Trinamic 24V electric motor (TRINAMIC Motion Control Hamburg, Germany) combined with an Arduino uno board (Arduino AG) was used to rotate it at 1 rad/s. The Polhemus tracking system was used to capture motion. Sensor 1 was located on the surface of the object and sensor 2 on a wooden table where the test object and cube reference system were located on top (Figure 3-16). Coordinates of sensor 2 must be constant in order to validate the experiment as disruption-free. The Polhemus system detects positions and orientation of the object during rotation. The data obtained was processed following the same steps explained in "3.2. Kinematic analysis", with the exception that in this case there is no change in the reference system since it is not a relative movement. FHA parameters (axis direction, axis position and quantity of translation around the axis) were estimated through the six algorithms using different angle steps (0.5°, 1°, 2°, 3°, 5°, 10°). The estimated value of these parameters was compared with the theoretical value. Angle error between the estimated and theoretical FHA direction was calculated, as well as the translation and position error in order to find the method with the least error.

The theoretical position and orientation of the axis of motion are constant throughout the entire rotation movement since the movement is supposed to be a planar rotation. The theoretical axis position was calculated by measuring the position of the disk center (before starting rotatory motion) with the Polhemus sensor pointer. Theoretical axis direction was obtained by measuring three non-collinear points on the disk surface with that pointer. The normal axis to these three points (which form a plane) coincides with the theoretical rotation axis of motion. Since the movement is a planar rotation, the quantity of translation along the axis is null.

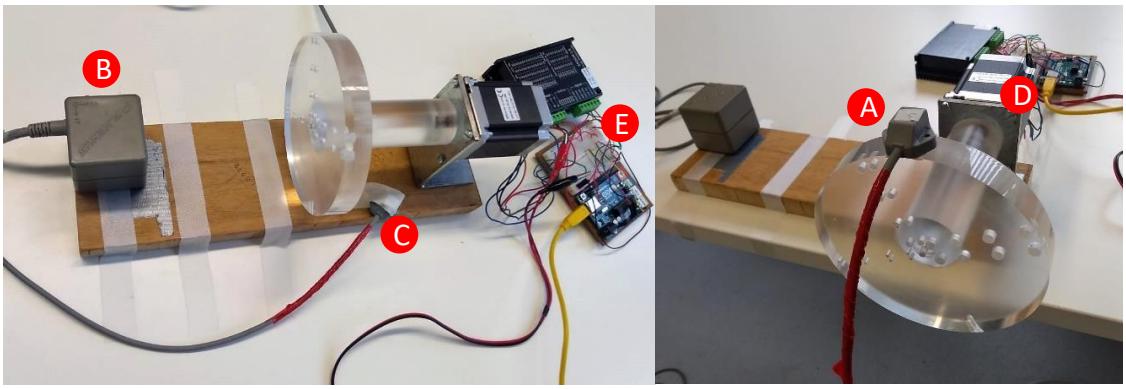

Figure 3-16 : Rotating test object. A) Sensor 1 fixed to the object test. B) Cube reference (0, 0, 0). C) Sensor 2 fixed to the wooden table where the test object is placed on top. D) Motor to rotate the object. E) Arduino Uno board.

3.4.2. Head movement simulation

The model simulates a rotation of 360° of a point around an axis parallel to the vertical axis and located 150 mm from the point without translation along it. In order to simulate a head movement, it was performed at a constant angular velocity of 1 rad/s. As mentioned above, Polhemus system has a resolution of 240 Hz. The simulation was performed under the same conditions. Relating angular velocity (1 rad/s) with tracking motion resolution (240 Hz) it is possible to reproduce head rotation movement as if it were acquired by Polhemus system, and the sampling frequency for movement simulation in MATLAB is obtained as follows:

1 s = 240 frames (Polhemus resolution, 240 Hz)

1 s = 180/π ° (angular velocity during head movement, 1 rad/s)

Which means that the relationship between frames and degrees is given by:

1 frame = (180/ π)/240 ° = (3/ π)/4 °

Consequently, the sampling interval T to discretize the signal is equal to $3/(4\,x\ \ \pi)$ so that sampling frequency is $f = 1/T$.

Since the MATLAB simulation is a planar movement it is possible to estimate the orientation of the point in the space (rotation matrix) during rotation due to the fact that there is no translation along the axis (Figure 3-17). This point simulates the movement of Polhemus Sensor 1 located on the forehead during data acquisition.

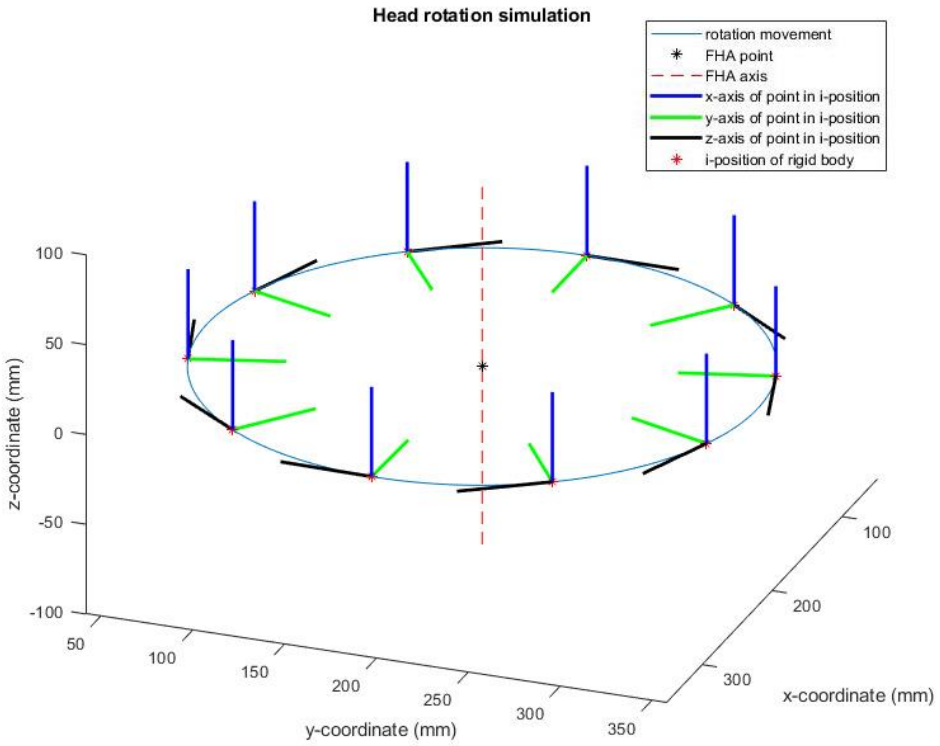

Figure 3-17: Head rotation simulation around the axis whose direction is equal to (0, 0, 1). Point positions during movement are located 150 mm from the axis and its orientation during movement is defined by the direction cosines (rotation matrix) of its x, y and z-axes.

However, this simulation describes an ideal rotation without error, which is not realistic for motion tracking systems because there is an error in the measurement of position and orientation. Some technology can be more accurate in orientation (e.g. electromagnetic sensor) and other in position (e.g. optical sensors) [6]. Therefore, it is required to introduce different levels of noise in position and orientation in order to be closer to a real situation. The process of introducing noise is similar that as followed by Cescon et al [6] by adding random Gaussian noise in the final position and orientation of the object. Gaussian noise is a basic noise model to mimic the effect of many random processes that occur in nature. It has a normal distribution and an average value of zero. Different noise levels, with different standard deviations, were introduced for orientation and position to the ideal movement. The methodology followed for each type of noise (in orientation and position) is detailed in the next paragraphs.

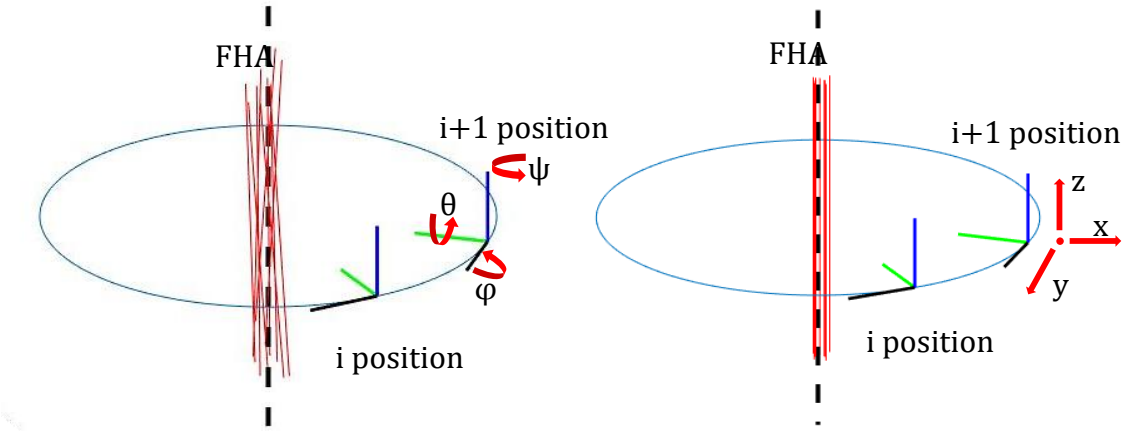

Figure 3-18: Effect of noise in position and orientation on FHA. A) Added orientation noise (φ, θ, ψ). B) Added position noise (x, y, z)

Orientation noise

Orientation noise was a vector of three components expressed in degrees normally distributed with a standard deviation of 0.1°, 0.5° and 1° for each level. Therefore, three noise levels were introduced. Each component of that vector represents an elemental rotation of the rigid body (defined by the position of the point and its rotation matrix, see Figure 3-17) around its direction cosines (x, y, z), what are known as Cardan angles. Those three rotations were performed using XYZ Cardan sequence, whose rotation matrix is defined by equation (49), where (φ, θ, ψ) are the components x, y and z of the added orientation noise.

$$R_{XYZ} \rightarrow \begin{pmatrix} cos\theta cos\psi & -cos\theta sin\psi & sin\theta \\ cos\varphi sin\psi + cos\psi sin\varphi sin\theta & cos\varphi cos\psi - sin\varphi sin\theta sin\psi & -cos\theta sin\varphi \\ sin\varphi sin\psi - cos\varphi cos\psi sin\theta & cos\psi sin\varphi + cos\varphi sin\theta sin\psi & cos\varphi cos\theta \end{pmatrix} \quad (49)$$

Given an angle step, the movement is divided into finite displacements. For each finite displacement (defined by initial and final position), that rotation matrix R_{XYZ} was multiplied to the original rotation matrix of the final position in order to achieve the new orientation. The six FHA calculation methods were applied to a total of 1000 displacements with orientation noise in final position for three different types of noise levels (0.1°, 0.5° and 1°). For each angle step (0.5°, 1°, 2°, 3°, 5°, 10°), a total of six super-matrices (once per method) with a length of $1000 \times m \times n$ were obtained, where m is the number of FHA parameters estimated (axis direction, axis position and quantity of translation) and n is the noise level (0.1°, 0.5° and 1° respectively).

Position noise

Position noise is also a vector of three components expressed in mm normally distributed with a standard deviation of 0.05mm, 1mm and 2mm (three noise levels). Each component of that vector represents the noise introduced in x, y and z-coordinates of the point position during movement. That noise is also introduced in the final position of a finite displacement. The methodology is the same as that followed for the orientation

noise: for each angle step (0.5°, 1°, 2°, 3°, 5°, 10°), a total of six super-matrices (once per method) with a length of $1000 \times m \times n$ were obtained, where m is the number of FHA parameters estimated (axis direction, axis position and quantity of translation) and n is the noise level (0.05mm, 1mm and 2mm).

A total of twelve datasets, six for added orientation noise and six for added position noise were obtained. The results of these datasets are detailed in the next chapter.

3.5. Statistical analysis

Statistical analysis is performed between the 12 datasets. For the rotating object test, a one-way analysis of variance is performed in order to determine whether the different FHA calculation methods have different effects on FHA parameters and to choose the least-error method, based on the mean and standard deviation of the error.

For the movement simulation in MATLAB, Kruskall-Wallis test is performed to evaluate the influence of adding different levels of noise on FHA calculation error. Influence of chosen angle step on FHA calculation is also evaluated. Significance level was set at α = 0.05.

3.6. Implementation of FHA analysis software

FHA analysis software was implemented in MATLAB and it processes cervical movement data acquired following the acquisition protocol explained above. As a result of the processing, all FHAs for the whole movement at a are displayed and it is possible to increase or decrease the angle step in order to analysis the movement in a more global way or focus on small displacements, respectively. As output variables, three parameters that depicts FHA behavior are obtained: mean angle (MA), mean distance (MD) and convex hull area (CH). Its efficacy as dispersion indexes were reported by previous studies [6][23][27] and their explanation is reported in “State-of-the-art” section. Figure 3-19 shows the processing of different head movements (flexion-extension, lateral bending and rotation) for different chosen angle steps. The FHA calculation algorithm implemented is the one chosen as the least error using the methodology explained above, which reasoning is explained in “Discussion” section.

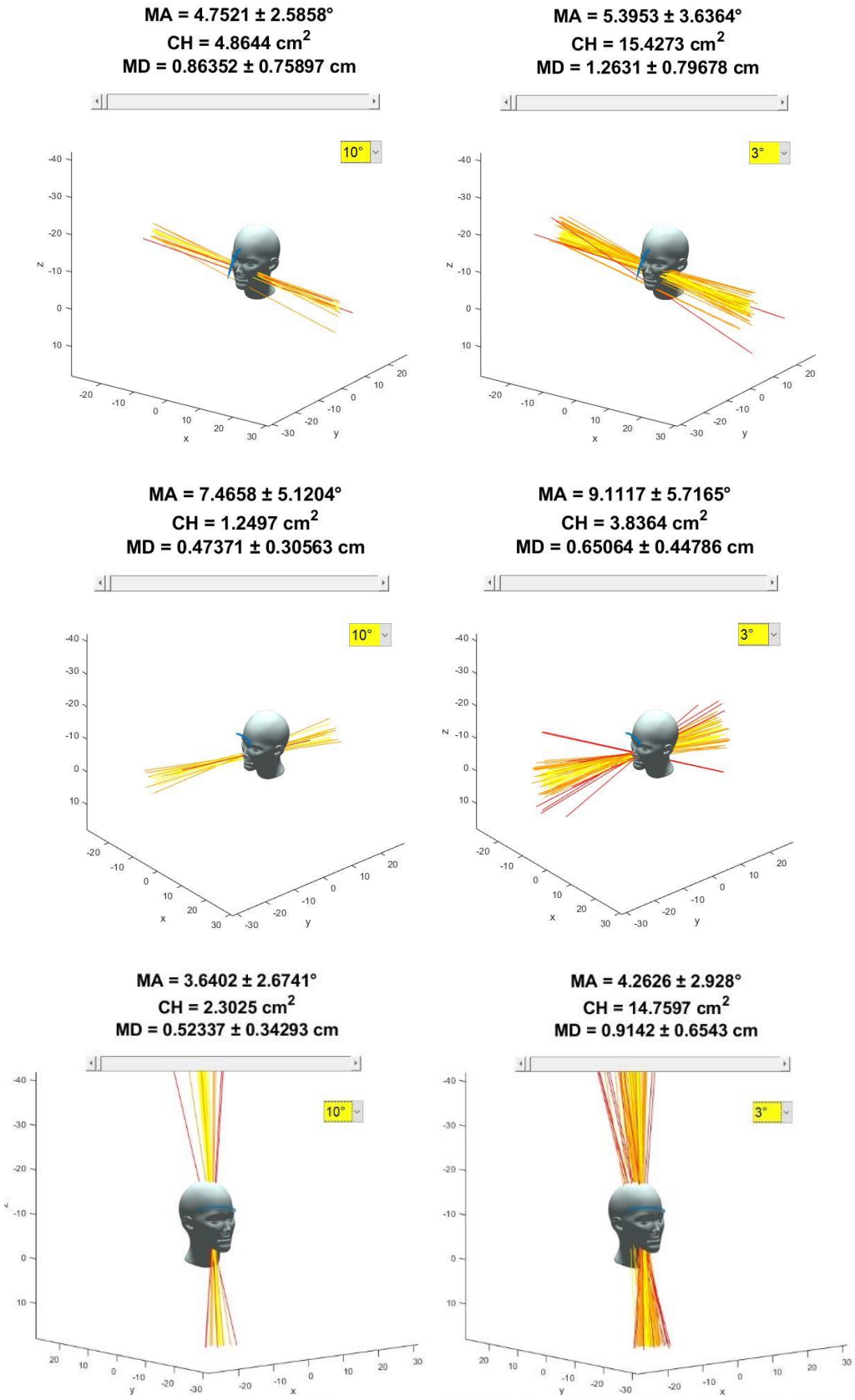

Figure 3-19: FHAs display for the same subject performing three types of head movement: flexion-extension, lateral bending and rotation. Results for different angle steps are shown. MA (mean angle), CH (convex hull area) and MD (mean distance) are shown. The blue dotted trajectory depicts the position of the sensor located on the forehead during motion.

Chapter 4

4. Results

4.1. Rotating object experiment

Quantitative results of translation, angle and position error for the six different methods are shown in Table 1 , Table 2 and Table 3, respectively. The algorithms were tested at different angle steps: 0.5°, 1°, 2°, 3°, 5° and 10°. Mean and standard deviation of each type of error were calculated. Translation and position error are measured in centimeters and angle error in degrees. Where FHA calculations became inconsistent, due to the impossibility of calculating its equation, were noted as '—'. This is produced as a result of mathematically undefined operations such as 0/0 or ∞-∞. For angle steps at 1° and 0.5°, only method 2 and method 5 were consistent for translation and angle error. Furthermore, method 3 started having problems in calculation at a 3° angle step. No method was fully consistent for position error calculation at 1° and 0.5° angle step. Those undefined operations (represented by NaN in MATLAB) for do not mean that FHA calculation for all finite displacements were inconsistent. For instance, at a 1° angle step method 3 has 1340 undefined operations for FHA calculation of a total of 2520 finite displacements. This fact is due to the combination of choosing a small angle step (< 2°) and movement discretization of tracking systems.

In order to determine whether FHA parameters error obtained from the different algorithms were significantly different, a one-way analysis of variance (ANOVA) was performed for each type of FHA error, taking translation, position and angle error as independent variables in each case, and the different methods as groups or levels of the analysis. For that case, undefined numerical results were not considered. The ANOVA was performed at 10° and 5° angle step. Results for angle step = 10° showed that method 3 in position axis error was significantly different ($p<0.05$) than the other methods (Figure 4-1). For angle step = 5°, an ANOVA analysis is performed without considered method 3 since the differences were evident for 10°. Results for 5° angle step (Figure 4-2) showed that method 2 was significantly different in axis position error. Furthermore, method 3 was also significantly different in angle error.

ROTATING OBJECT MOVEMENT							
Translation error (mean and standard deviation), cm							
Angle step	μ	**M1**	**M2**	**M3**	**M4**	**M5**	**M6**
	σ						
10	μ	0.09	0.09	0.09	0.09	0.09	0.10
	σ	0.07	0.07	0.07	0.07	0.07	0.07
5	μ	0.05	0.05	0.05	0.05	0.05	0.05
	σ	0.03	0.03	0.03	0.03	0.03	0.04
3	μ	0.03	0.03	--	0.03	0.03	0.03
	σ	0.02	0.02	--	0.02	0.02	0.02
2	μ	0.02	0.02	--	0.02	0.0	0.02
	σ	0.01	0.01	--	0.01	0.01	0.01
1	μ	--	0.01	--	--	0.01	--
	σ	--	0.01	--	--	0.01	--
0.5	μ	--	0.01	--	--	0.01	--
	σ	--	0.01	--	--	0.01	--

Table 1: Mean (μ) and standard deviation (σ) of translation error for the six methods with the rotating object experiment.

ROTATING OBJECT MOVEMENT							
Angle error (mean and standard deviation), degrees							
Angle step	μ	**M1**	**M2**	**M3**	**M4**	**M5**	**M6**
	σ						
10	μ	5.80	5.80	5.84	5.80	5.80	5.90
	σ	2.87	2.86	3.00	2.86	2.86	2.83
5	μ	5.84	5.84	6.53	5.84	5.84	5.80
	σ	2.89	2.88	2.96	2.88	2.88	2.79
3	μ	5.94	5.92	--	5.93	5.93	5.84
	σ	2.92	2.91	--	2.91	2.91	2.79
2	μ	6.00	5.97	--	5.98	5.98	5.87
	σ	2.95	2.94	--	2.95	2.95	2.83
1	μ	--	19.68	--	--	31.76	--
	σ	--	23.43	--	--	30.87	--
0.5	μ	--	27.44	--	--	46.73	--
	σ	--	26.29	--	--	29.97	--

Table 2: Mean (μ) and standard deviation (σ) of angle error for the six methods with the rotating object experiment.

ROTATING OBJECT MOVEMENT							
Position error (mean and standard deviation), cm							
Angle step	μ	**M1**	**M2**	**M3**	**M4**	**M5**	**M6**
	σ						
10	μ	1.02	1.03	1.31	1.02	1.02	1.01
	σ	0.42	0.43	0.82	0.42	0.42	0.42
5	μ	1.03	1.10	4.24	1.03	1.03	1.02
	σ	0.43	0.49	13.67	0.43	0.43	0.43
3	μ	1.05	2.13	--	1.05	1.05	1.04
	σ	0.46	6.77	--	0.46	0.46	0.45
2	μ	1.06	3.38	--	1.06	1.06	1.05
	σ	0.48	10.62	--	0.48	0.48	0.47
1	μ	--	--	--	--	--	--
	σ	--	--	--	--	--	--
0.5	μ	--	--	--	--	--	--
	σ	--	--	--	--	--	--

Table 3: Mean (μ) and standard deviation (σ) of position error for the six methods with the rotating object experiment.

ANGLE STEP = 10 °

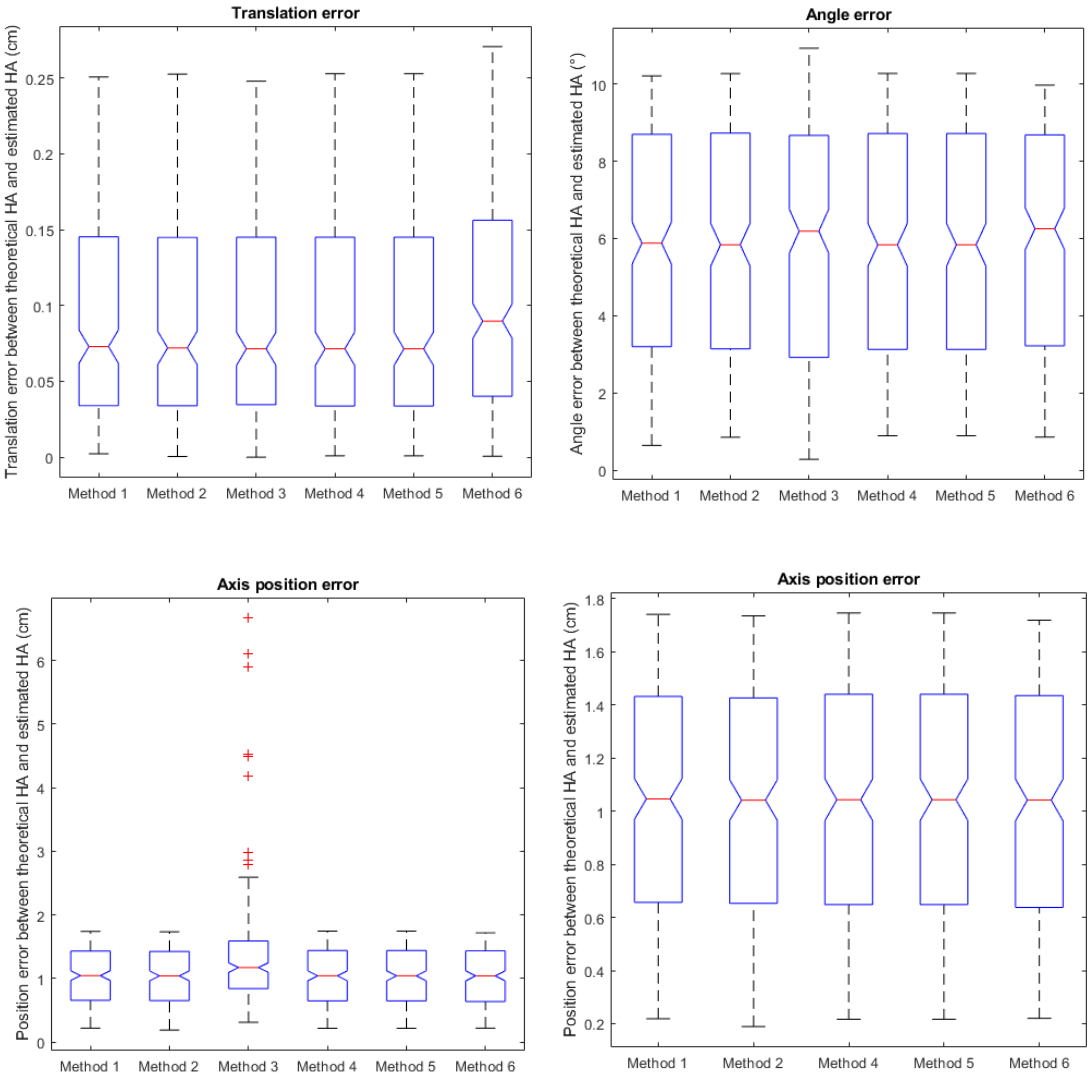

Figure 4-1: Boxplot of translation, position and angle error for the six implemented method at an angle step of 10°.

ANGLE STEP = 5 °

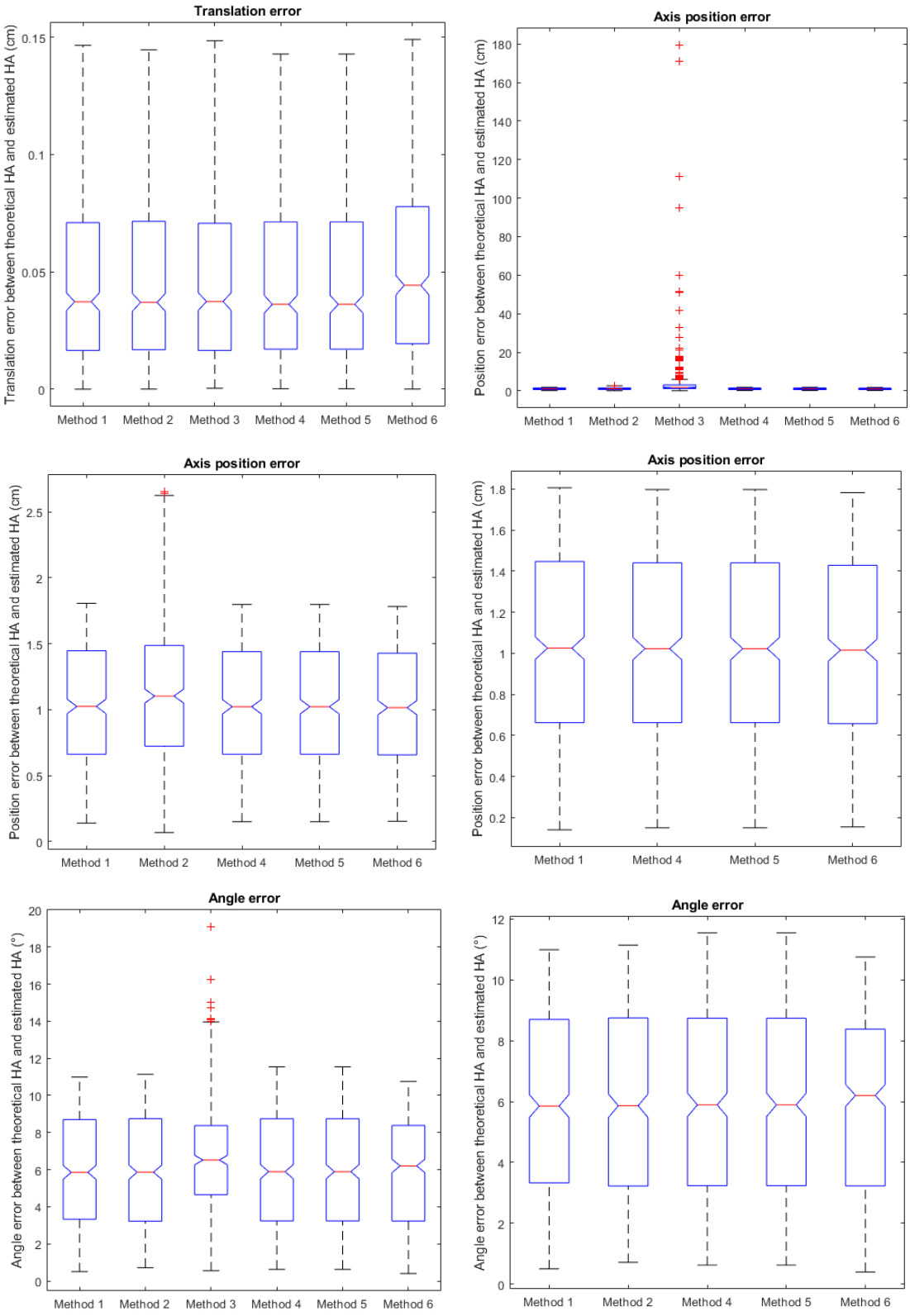

Figure 4-2: Boxplot of translation, position and angle error for the six implemented method at an angle step of 5°.

4.2. MATLAB movement simulation

No differences on quantitative results were found between the six methods for the MATLAB movement simulation so the aim of this experiment is to evaluate the effect of angle step on FHA calculation by applying the least error method based on the results obtained in the rotating object test. Method 5 (based on single value decomposition algorithm) was chosen as the least error prone. This decision is detailed in Chapter 5. Discussion. From now on, results of FHA estimations for the MATLAB simulation using method 5 are presented.

Kruskall-Wallis test was performed to the simulations in order to evaluate the influence of angle step on angle, position and translation error. Kruskal Wallis is a non-parametric method that will report if there is a significant difference in angle, position and translation error between different angle steps (0.5°, 1°, 2°, 3°, 5°, 10°). Significance level was set at $\alpha = 0.05$. The test was performed to two simulations: with 1 mm noise in position and 1° noise in orientation. The analysis showed proportional relationship between angle step and error in FHA position and angle ($p<0.001$). No relation between angle step and translation error was found ($p=0.938$). The error in the three parameters increased proportionally with the noise level. Figure 4-3 shows the effect of noise and angle step in FHA calculation error. Table 4 and Table 5 show mean and standard deviation of FHA error for added noise in position and orientation respectively.

MATLAB SIMULATION WITH POSITION NOISE							
	Noise level (mm)	ANGLE STEP					
TYPE OF ERROR	0.05	0.5°	1°	2°	3°	5°	10°
	1						
	2						
TRANSLATION (mm)	μ	0.04	0.04	0.04	0.04	0.03	0.04
	σ	0.03	0.03	0.03	0.03	0.03	0.03
	μ	0.80	0.80	0.80	0.78	0.83	0.81
	σ	0.61	0.63	0.60	0.57	0.64	0.61
	μ	1.61	1.67	1.56	1.62	1.62	1.50
	σ	1.21	1.26	1.23	1.22	1.22	1.17
POSITION (mm)	μ	7.55	3.76	1.91	1.20	0.75	0.36
	σ	3.84	1.95	0.99	0.64	0.39	0.19
	μ	150.31	73.93	38.63	25.80	15.11	7.28
	σ	75.48	38.57	19.27	13.43	7.72	3.92
	μ	300.80	151.98	77.27	49.51	29.63	14.15
	σ	158.75	78.35	41.27	25.72	15.29	7.66
ANGLE (°)	μ	0	0	0	0	0	0
	σ	0	0	0	0	0	0
	μ	0	0	0	0	0	0

	σ	0	0	0	0	0	0
	μ	0	0	0	0	0	0
	σ	0	0	0	0	0	0

Table 4: Mean and standard deviation of angle, position and translation error for the MATLAB simulation with added noise in position

MATLAB SIMULATION WITH ORIENTATION NOISE							
	Noise level (°)	ANGLE STEP					
TYPE OF ERROR	0.1	0.5°	1°	2°	3°	5°	10°
	0.5						
	1						
TRANSLATION (mm)	μ	0.20	0.20	0.21	0.21	0.21	0.22
	σ	0.16	0.15	0.16	0.16	0.16	0.17
	μ	0.56	0.88	0.95	1.00	1.05	1.04
	σ	0.35	0.61	0.73	0.75	0.77	0.81
	μ	0.60	1.15	1.81	1.93	2.08	2.07
	σ	0.35	0.70	1.21	1.42	1.64	1.57
POSITION (mm)	μ	25.98	11.78	6.51	4.11	2.52	1.27
	σ	20.47	8.85	4.67	3.23	1.92	0.98
	μ	100.73	70.23	34.90	21.10	13.01	6.25
	σ	77.99	84.38	29.77	17.29	10.38	4.71
	μ	110.85	98.44	67.38	45.97	26.44	12.24
	σ	45.63	61.04	65.82	53.92	23.43	8.90
ANGLE (°)	μ	14.94	7.35	3.83	2.54	1.51	0.75
	σ	8.03	3.74	2.02	1.28	0.79	0.39
	μ	49.02	36.35	18.45	12.59	7.48	3.69

	σ	22.31	20.10	10.50	6.56	4.03	1.93
	μ	55.38	49.39	35.58	24.39	15.36	7.45
	σ	22.21	22.23	19.33	14.03	8.37	3.82

Table 5: Mean and standard deviation of angle, position and translation error for the MATLAB simulation with added noise in orientation.

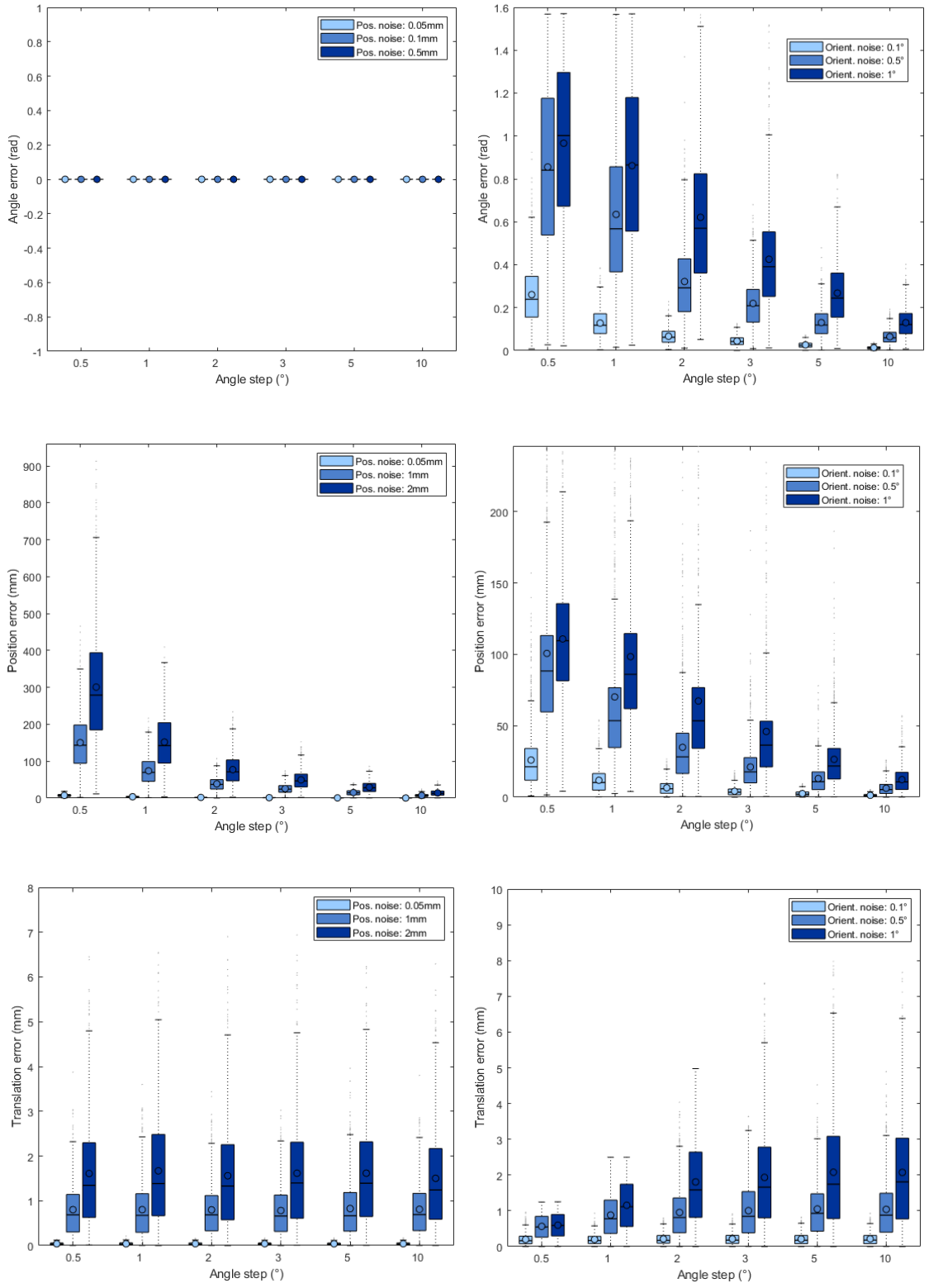

Figure 4-3: Effect of introducing position (left boxplots) and orientation (right boxplots) noise on FHA parameters: angle error (first row), position error (second row) and translation error (third row).

Chapter 5

5. Discussion

5.1. FHA calculation method with least error

Results obtained from the rotating object experiment are analyzed and used to decide which is the algorithm that provide the minimum error prone. FHA was calculated trough the different methods for each displacement which depends on the angle step. Six different angle steps (0.5°, 1°, 2°, 3°, 5°, 10°) were evaluated for the whole movement in order to evaluate its effect on FHA error. As it was mentioned, the stochastic error is inversely to the displacement between the initial and final position.

At 10° and 5° angle step, error in FHA calculation is very similar for all methods so it is required to evaluate the error at smaller angle steps because this is when differences between methods become more evident since the error in FHA calculation increases. Only method 2 (displacement transformation matrix method) and method 5 (single value decomposition method) are consistent in FHA calculation for all angle steps. At smaller angles, the accuracy of the sensors has a determining role because the error introduced by the sensors may lead to an identical value of initial and final position and orientation. That fact causes a mathematically undefined operation in the resolution of some algorithms. For instance, resolution of method 3 implies the calculation of the inverse of the matrix determined by the displacement between initial and final position. With very small displacements that matrix is singular or close to being so, and as a result its inverse cannot be calculated.

By analyzing the results obtained for the translation error by method 2 and 5, same mean and standard deviation values are obtained. As for the angle error, the differences between both methods are noticed at angle step equal to 1°, being the error at that angle step of for method 2: 19.68 ± 23.43° and for method 5: 31.76 ± 30.87°. For the position error, at an angle step of 5° there is a slight difference in both methods: 1.10 ± 0.49 cm for method 2 and 1.03 ± 0.43 cm for method 5. That small difference in position error increases at 3° angle step, being 2.13 ± 6.77 cm for method 2 and 1.05 ± 0.46 cm for method 5. Although better results with method 2 are found for angle error, the values for position error are prioritized when deciding the most effective FHA calculation method. This is because the differences between both methods for position error are found at an angle step greater than for the angle error, which means smaller stochastic error. As a result of this

reasoning, method 5, based on single value decomposition algorithm, is chosen as the least error prone.

5.2. Effect of adding noise on FHA estimations

For the MATLAB simulation, different noise levels were added in positions and orientations. These levels have a different effect on the error of the FHA calculation. The added noise simulates the measurement error of the motion capture sensors. The accuracy of the sensor depends on the technology used. As it was mentioned, some technology can be more accurate in orientation (e.g. electromagnetic sensors) and other in position (e.g. optical sensors) [6], so FHA error may change depending on the technology used for motion capturing. Analyzing the results of mean and standard deviation for FHA error (Table 4 and Table 5), it can be observed that orientation noise has a greater effect on FHA calculation error. For instance, at an angle step of 10°, 1 mm level of noise position introduces 7.28 ± 3.92 mm error in FHA position and 0.81 ± 0.61 mm error in FHA translation, while the error in angle is null. On the other hand, 1° level of orientation noise introduces 12.24 ± 8.90 mm error in FHA position, 2.07 ± 1.57 mm error in translation and 7.45 ± 3.82° error in angle. It is therefore reasoned that to use the FHA approach it is more convenient to use a motion capture system with greater accuracy in orientation since measurement orientation error has more impact on FHA error than measurement position error.

5.3. Effect of angle step on FHA estimations

As it is reported in Chapter 4: Results, the FHA error increases as the angle step decreases. That is why for the six algorithms, FHA was calculated at different angle steps in order to find the least error prone method. Trough the experiment of the rotating object, method 5 was chosen as the most optimal. Next, the MATLAB simulation was performed using method 5 at different noise levels and angle steps. The results show higher position and angle error at small displacements, especially when the noise level was added in orientation. That results are compared with a previous study [6] that also performed a simulation with added Gaussian noise to evaluate the effect of angle step on FHA calculation error. In the study of Cescon at. the algorithm method to calculate FHA was trough the rotation matrix but it was not reported by which algorithm the rotation matrix was reached. The results of adding 0.1° and 0.5° in orientation noise were compared between the present study and the results obtained by Cescon et al (Figure 5-1 and Figure 5-2). However, this author does not specify the methodology used to introduce the orientation noise, so the comparison cannot be one hundred percent reliable. For the present study Cardan angles with XYZ sequence were used, as it was reported in the chapter “Materials and Methods”. Anyway, similar values were achieved for angle (Figure 5-1) and position (Figure 5-2) error at different angle steps. For each figure, the error values for the same orientation noise and angle step are identified in the study of Cescon and in the present study with the same label number. The values obtained for the present study were slightly smaller in position error than the study of Cescon et al, which

is due to the optimisation of the FHA estimations performed trough the rotating test object since the least error prone algorithm was chosen as the standard method for FHA calculation.

Results from Cescon et al **Results from the present study**

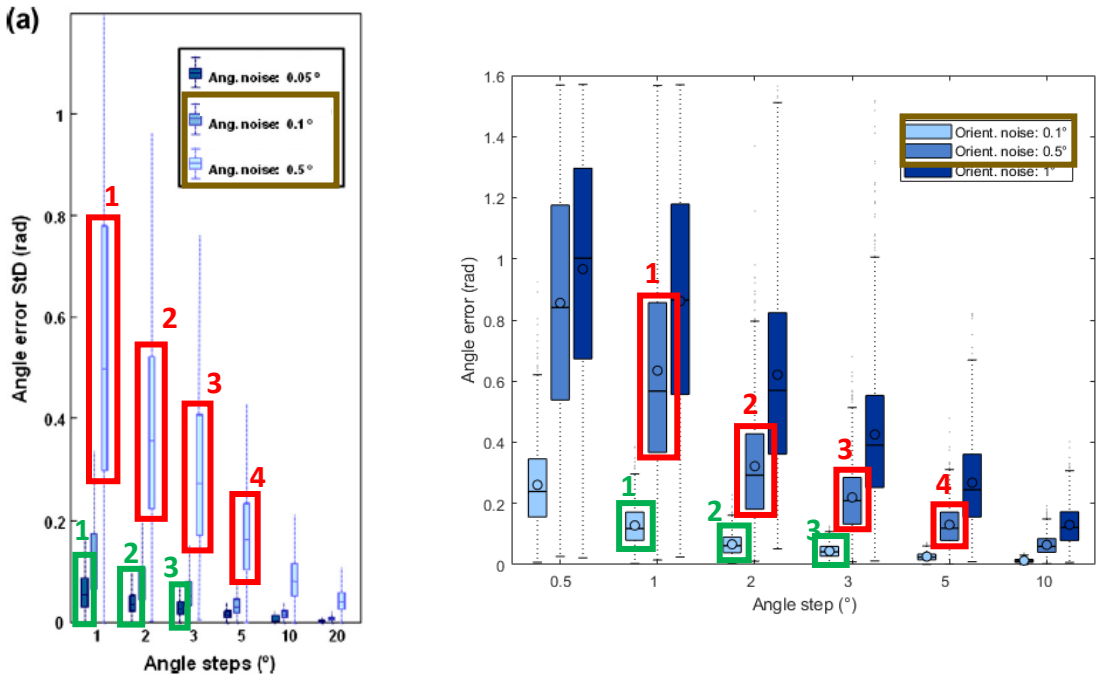

Figure 5-1: Comparison of the effect of angle step on FHA estimation between the present study and the study of Cescon et al. Results for angle error.

Results from Cescon et al **Results from the present study**

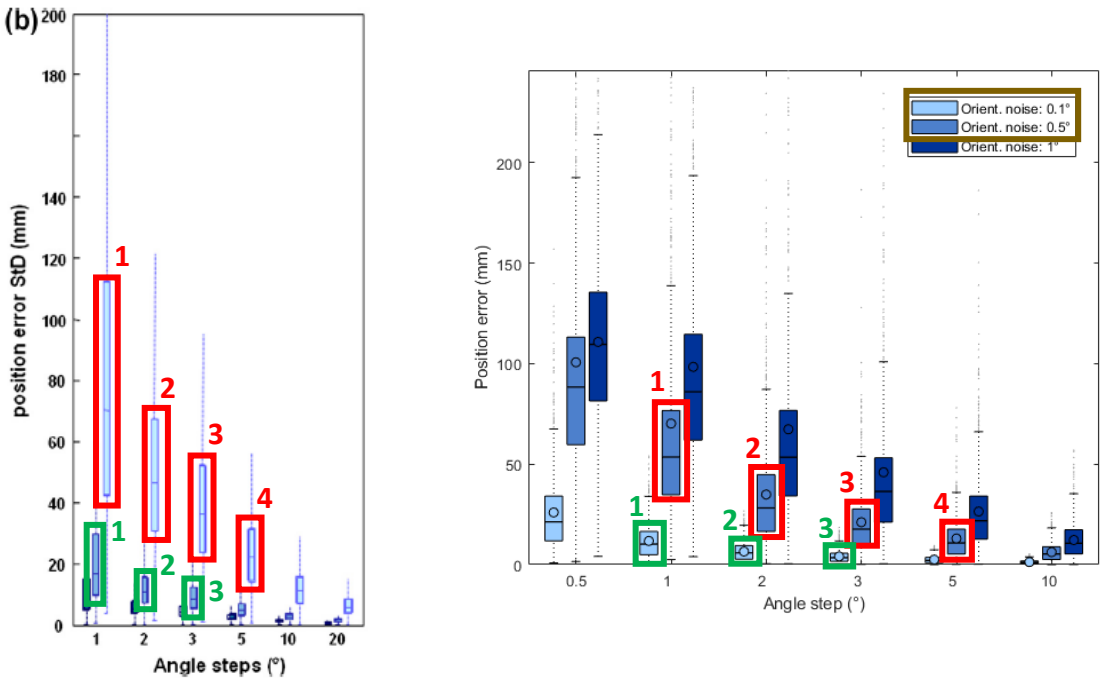

Figure 5-2: Comparison of the effect of angle step on FHA estimation between the present study and the study of Cescon et al. Results for position error.

5.4. Limitations of the study

The dataset registration of cervical movement only used one sensor attached to the head in order to describe cervical movement. As a result, its position (x, y, z coordinates) and orientation (rotation matrix) are recorded. For some FHA calculation algorithms that need the final and initial position of at least three points to perform its equation, these are estimated constructing three points from the sensor position and its rotation matrix. That means that the three estimated points accumulate the measurement error of the position of the sensor, added to the error in its measured orientation. The post-processing tries to remove this error, but good results would be found for FHA calculation if the number of sensors attached to the head (considered as a rigid body) was higher.

It is also important to notice that the rotating object experiment was performed by using a motor to undergo rotation. This movement may cause distortion to the position and orientation recorded by the sensor attached to the object surface, as electromagnetic sensors are sensitive to vibrations. The values of distortion obtained in the Polhemus software showed no signs of disturbance, but it is easy to reason that the movement of the motor had influenced on the position and orientation values.

5.5. Suggestions for future work

The present work can be improved in different ways. One could be applying Bayes' theorem in order to obtain the probability of obtaining FHA-parameters for different angle steps based on prior knowledge of position and orientation. That study will show at which displacements the FHA calculation are least error prone.

A second way could be to analyse head movement data recorded by using more than one sensor attached on the head. This would reduce the error in FHA calculation and would avoid the estimation of the position of three points more from the orientation matrix. Using another tracking system that relies on tracing the position of markers would be another interesting way to overcome this issue.

Chapter 6

6. Conclusion

Although 6 DOF approach to analysis human movement is widely used among clinicians, it introduces problems in the reliability of the results while comparing between patients due to the chosen reference dependence. The FHA approach solves this dependence problem [6]. However, it struggles with problems related with calculation error and poor visualization techniques.

In this thesis, a rotating object test was performed in order to optimize FHA estimation. The rotation movement was recorded by using Polhemus tracking system. Six different FHA calculation methods [32][33][34][35][36][37] were applied to this movement and parameters such as axis position, axis direction and quantity of translation around the axis were obtained for each method and compared with the theoretical values. Different angle steps were tested for FHA calculation. Comparison between the estimated and theoretical FHA parameters determined that FHA calculation method which obtains the rotation matrix (corresponding to the displacement) through the Single Value Decomposition algorithm (SVD) is the least error prone method.

Once the FHA calculation method was optimized, a head movement simulation was performed in MATLAB and different levels of noise in position and orientation were added. FHA was calculated for different angle steps in order to evaluate the effect of added noise. These levels of noise represent the error measurement of the tracking systems. As a result, it was obtained that added orientation noise had more influence on FHA error than added position noise which leads to prioritizing the accuracy in orientation rather than position in a motion capture system. The effect of chosen angle step was also evaluated showing proportional inversely between FHA error and angle step, coinciding with previous studies [6]. The optimisation of FHA estimations through which the least error prone method is chosen makes FHA approach a promising method between clinician to analyse human movement. Parameters such as MA, MD and CH are used to quantify FHA behavior of a head movement [6][23][27]. Those parameters that describe the dispersion of FHA promise to be a good metric to quantify joint functionality that can help clinicians to detect cervical abnormalities.

Bibliography

[1] Lu, Tung-Wu & Chang, Chu-Fen. (2012). Biomechanics of human movement and its clinical applications. The Kaohsiung journal of medical sciences. 28. S13-25. 10.1016/j.kjms.2011.08.004.

[2] Kinerd, Nicholas, "Motion Capture Study of Human Movement Recognition" (2012). All Theses. 1512.

[3] Advanced Realtime Tracking. Motion Capture with ART-Human. Retrieved from https://ar-tracking.com/applications/motion-capture/

[4] An, Kai-Nan & Y Chao, E. (1984). Kinematic analysis of human movement. Annals of biomedical engineering. 12. 585-97. 10.1007/BF02371451.

[5] Fernández Villán, Alberto & Usamentiaga, Rubén & Carús Candás, Juan & Casado, Ruben. (2016). Driver Distraction Using Visual-Based Sensors and Algorithms. Sensors. 16. 1805. 10.3390/s16111805.

[6] Cescon, C., Cattrysse, E., Barbero, M., 2014. Methodological analysis of finite helical axis behavior in cervical kinematics. Journal of Electromyography and Kinesiology 24, 628–635. doi:10.1016/j.jelekin.2014.05.004

[7] Dugailly, Pierre-Michel & Stéphane, Sobczak & Sholukha, Victor & Van Sint Jan, Serge & Salvia, Patrick & Feipel, Veronique & Rooze, Marcel. (2009). In vitro 3D-kinematics of the upper cervical spine: Helical axis and simulation for axial rotation and Xexion extension. Surgical and radiologic anatomy : SRA. 32. 141-51. 10.1007/s00276-009-0556-1.

[8] Grip, Helena & Hager, Charlotte. (2013). A new approach to measure functional stability of the knee based on changes in knee axis orientation. Journal of biomechanics. 46. 10.1016/j.jbiomech.2012.12.015.

[9] Raquel Urtasun. Human Motion Analysis. Lecture 2: Human Body Representations. TTI Chicago. Retrieved from https://www.cs.toronto.edu/~urtasun/courses/ETH10/lecture2.pdf

[10] Woltring, H.J. & Huiskes, R & de Lange, A & Veldpaus, F.E.. (1985). Finite Centroid and Helical Axis Estimation from Noisy Landmark Measurements in the Study of Human Joint Kinematics. Journal of biomechanics. 18. 379-89. 10.1016/0021-9290(85)90293-3.

[11] Anthony G Schache, Tim V Wrigley, Peter D Blanch, Roland Starr, David A Rath, Kim L Bennell, The effect of differing Cardan angle sequences on three dimensional lumbo-pelvic angular kinematics during running, Medical Engineering & Physics, Volume 23, Issue 7, 2001, Pages 495-503.

[12] Chapter 11. Angular Kinematics of Human Movement. In: Hall SJ. Hall S.J. Ed. Susan J. Hall.eds. Basic Biomechanics, 5e New York, NY: McGraw-Hill; 2007.

[13] Vikne H, Bakke ES, Liestøl K, Engen SR, Vøllestad N. Muscle activity and head kinematics in unconstrained movements in subjects with chronic neck pain;

cervical motor dysfunction or low exertion motor output?. BMC Musculoskelet Disord. 2013;14:314. Published 2013 Nov 4. doi:10.1186/1471-2474-14-314

[14] Reynolds, H. M., & Hubbard, R. P. (1980). Anatomical Frames of Reference and Biomechanics. Human Factors, 22(2), 171–176. Retrieved from https://doi.org/10.1177/001872088002200205

[15] Cattin, Emanuele & Roccella, S & Vitiello, Nicola & Sardellitti, Irene & Artemiadis, Panagiotis & Vacalebri, Pierpaolo & Vecchi, Fabrizio & Carrozza, Maria Chiara & Kyriakopoulos, Kostas & Dario, Paolo. (2008). Design and Development of a Novel Robotic Platform for Neuro-Robotics Applications: the NEURobotics ARM (NEURARM).. Advanced Robotics. 22. 3-37.

[16] Kettler, F. Marin, G. Sattelmayer, M. Mohr, H. Mannel, L. Dürselen, L. Claes, H. J. Wilke. Finite helical axes of motion are a useful tool to describe the three-dimensional in vitro kinematics of the intact, injured and stabilised spine. Eur Spine J. 2004 Oct; 13(6): 553–559. Published online 2004 May 18. doi: 10.1007/s00586-004-0710-8

[17] R. Karduna, Andrew & Mcclure, Philip & Michener, Lori. (2000). Scapular kinematics: Effects of altering the Euler angle sequence of rotations. Journal of biomechanics. 33. 1063-8. 10.1016/S0021-9290(00)00078-6.

[18] Baudet A, Morisset C, d'Athis P, et al. Cross-talk correction method for knee kinematics in gait analysis using principal component analysis (PCA): a new proposal. PLoS One. 2014;9(7):e102098. Published 2014 Jul 8. doi:10.1371/journal.pone.0102098

[19] Young-Hoo Kwon, 1998- Helical (Screw) Axis. Retrieved from http://www.kwon3d.com/theory/jkinem/helical.html

[20] Hakim Mecheri. Estimation de l'axe hélicoïdal fini et instantané à partir de Données cinématiques: étude comparative. Université du Quebec. Published 2005 April 20.

[21] Marco Barbero, Deborah Falla, Ron Clijsen, Filippo Ghirlanda, Alessandro Schneebeli, Markus J. Ernst, Corrado Cescon, Can parameters of the helical axis be measured reliably during active cervical movements?, Musculoskeletal Science and Practice, Volume 27, 2017, Pages 150-154, ISSN 2468-7812, https://doi.org/10.1016/j.math.2016.10.008.

[22] Frances T. Sheehan, The finite helical axis of the knee joint (a non-invasive in vivo study using fast-PC MRI), Journal of Biomechanics, Volume 40, Issue 5, 2007, Pages 1038-1047.

[23] Federico Temporiti, Roberta Furone, Corrado Cescon, Marco Barbero, Roberto Gatti, Dispersion of helical axes during shoulder movements in young and elderly subjects, Journal of Biomechanics, Volume 88, 2019, Pages 72-77.

[24] Feras Alsultan, Corrado Cescon, Alessandro Marco De Nunzio, Marco Barbero, Nicola R. Heneghan, Alison Rushton, Deborah Falla, Variability of the helical axis during active cervical movements in people with chronic neck pain, Clinical Biomechanics, Volume 62, 2019, Pages 50-57

[25] Técnicas avanzadas de análisis biomecánico. Instituto de Biomecánica de Valencia (IBV). Material class.

[26] Arin M. Ellingson, David J. Nuckley, Altered helical axis patterns of the lumbar spine indicate increased instability with disc degeneration, Journal of

Biomechanics, Volume 48, Issue 2, 2015, Pages 361-369, ISSN 0021-9290, https://doi.org/10.1016/j.jbiomech.2014.11.010.

[27] Cescon, Corrado & Barbero, Marco & Conti, Marco & Bozzetti, Francesco & Lewis, Jeremy. (2019). Helical axis analysis to quantify humeral kinematics during shoulder rotation. International Biomechanics. 6. 1-8. 10.1080/23335432.2019.1597642.

[28] Arin M. Ellingson, Vishal Yelisetti, Craig A. Schulz, Gert Bronfort, Joseph Downing, Daniel F. Keefe, David J. Nuckley, Instantaneous helical axis methodology to identify aberrant neck motion, Clinical Biomechanics, Volume 28, Issue 7, 2013, Pages 731-735, ISSN 0268-0033, https://doi.org/10.1016/j.clinbiomech.2013.07.006.

[29] Marco Barbero, Deborah Falla, Ron Clijsen, Filippo Ghirlanda, Alessandro Schneebeli, Markus J. Ernst, Corrado Cescon, Can parameters of the helical axis be measured reliably during active cervical movements?, Musculoskeletal Science and Practice, Volume 27, 2017, Pages 150-154, ISSN 2468-7812, https://doi.org/10.1016/j.math.2016.10.008.

[30] Feras Alsultan, Corrado Cescon, Alessandro Marco De Nunzio, Marco Barbero, Nicola R. Heneghan, Alison Rushton, Deborah Falla, Variability of the helical axis during active cervical movements in people with chronic neck pain, Clinical Biomechanics, Volume 62, 2019, Pages 50-57, ISSN 0268-0033, https://doi.org/10.1016/j.clinbiomech.2019.01.004.

[31] Venegas-Toro, W.; Page Del Pozo, AF.; Zambrano, I.; Ruiz, C. (2018). Análisis del eje instantáneo de rotación del movimiento de flexo-extensión del cuello mediante video análisis: fiabilidad y análisis de errores. 3C Tecnología. 7(1):79-92. https://doi.org/10.17993/3ctecno.2018.v7n1e25.79-92

[32] D'Alessio, Jerry & Russell, Kevin & Sodhi, Raj. (2015). On the application of the rodrigues displacement equation for the generation of finite helical axes for tibial motion. Journal of Biomechanical Science and Engineering. 10. 10.1299/jbse.15-00409.

[33] Page, Alvaro & De Rosario, Helios & Mata, Vicente & Atienza, Carlos. (2009). Experimental Analysis of Rigid Body Motion. A Vector Method to Determine Finite and Infinitesimal Displacements From Point Coordinates. Journal of Mechanical Design. 131. 031005. 10.1115/1.3066468.

[34] Inge Söderkvist, Per-Åke Wedin, Determining the movements of the skeleton using well-configured markers, Journal of Biomechanics, Volume 26, Issue 12, 1993, Pages 1473-1477, ISSN 0021-9290, https://doi.org/10.1016/0021-9290(93)90098-Y.

[35] J. S. Beggs, "Chapitre 3," in Kinematics: Hemisphere, Springer Verlag, 1983, pp. 41-47.

[36] Markley, F. L., Attitude determination using vector observations: A fast optimal matrix algorithm, Journal of the Astronautical Sciences 41(2) 261-280 (1993).

[37] B. K. P. Horn, "Closed Form Solution of Absolute Orientation Using Unit Quaternion," Optical Society of America, vol. 4, pp. 629-642, 1987.

[38] LIBERTY User Manual. 240/8 & 240/16. October 2005. Alken, Inc., dba Polhemus. Colchester, Vermont, U.S.A.

[39] A Page, P Candelas and F Belmar. On the use of local fitting techniques for the analysis of physical dynamic systems. European Journal of Physics, 27 (2006), pp. 273-279.
[40] The Basics of Basis Functions. Functional Data Analysis. Retrieved from http://www.psych.mcgill.ca/misc/fda/ex-basis-a1.html

Appendix

The MATLAB code of the three main functions are detailed in this section. “simulation_orientation_noise” and “simulation_position_noise” correspond to the functions that perform the simulations with added noise in orientation and position, respectively. “FHA_program” is the software that analyses FHA behavior. Each function has in turn calls to different functions, the purpose of which is explained.

SIMULATION - ADDED NOISE IN ORIENTATION

```
function [M1,M2,M3,M4,M5,M6]= simulation_orientation_noise(num_sim, step1)

%num_sim=1000; % NUMBER OF SIMULATION

%step1 -> angle step
M1=zeros(num_sim,8); %row=number of simulations ; column=FHA parameters to evaluated the
error
M2=zeros(num_sim,8);
M3=zeros(num_sim,8);
M4=zeros(num_sim,8);
M5=zeros(num_sim,8);
M6=zeros(num_sim,8);

[cbs_ideal,cbs2_ideal,cbs3_ideal,cbs4_ideal,RM2_ideal]=simulation(); % ideal movement.
Simulation creates an ideal rotation movement around and axis

(rotation) free noise
% noise levels: position -> 0.05, 0.1, 0.2
%               angle -> 0.1 0.5 1
% STEP
    %step1=10;
    num_ha=360/step1;
    interval= [1:floor(length(cbs_ideal)/num_ha):length(cbs_ideal)];
    interval=interval(:,floor(length(interval)/8):(floor(length(interval)/8)+1));

cbs_i=cbs_ideal(interval,:); % coordinates point 1
cbs2_i=cbs2_ideal(interval,:); % coordinates point 2
cbs3_i=cbs3_ideal(interval,:); % coordinates point 3
cbs4_i=cbs4_ideal(interval,:); % coordinates point 4
RM2_i=RM2_ideal(:,:,interval); % orientation of the rigid body in space
%points 1, 2, 3 and 4 belong to the rigid body

angle=[ 0.1 0.5 1];

for i=1:(length(angle)) % 3 levels of noise for the orientation
ang=angle(1,i);
for j=1:num_sim


% ADDED ERROR IN ANGLE
man=0; % angle mean, gaussian noise
[error_angles]=added_angle(cbs_i,ang, man); % this function creates a vector of three
elements. random gaussian noise
[Rmat,RM2_new,cbs2,cbs3,cbs4]=cardian_angles(RM2_i,error_angles,cbs_i); % this function
performs the rotation around the x,y,z axes using cardan angles
cbs=cbs_i; % the position of the first point does not change
% it only changes the orientation.

% RM2_new rotation matrix of each position
% Rmat rotation matrix (Cardan angles)
% simulation points -> cbs, cbs2, cbs3, cbs4
% u_1 -> axis direction
% theta_1 -> rotation angle around the axis (x, y, z)
% mfi_1 -> rotation angle (norm)
% p_1 -> point in the axis
% q -> vector of translation around the axis
```

```
% qt -> quantity of translation
RM2=RM2_new;
interval=[ 1 2 ];

[K_rodri,u_1,theta_1,mfi_1,p_1,q_1,qt_1]=method1_vector(cbs,cbs4,cbs3,cbs2,interval);
[u_2,mfi_2,q_2,p_2,qt_2,RM_m2]=method2_rotmatrix(RM2,interval,cbs,cbs2,cbs3,cbs4);
[mfi_4,Om_rodri,theta_4,u_4, p_4, qt_4, q_4
]=method4_rodriVirtualBody(cbs,cbs2,cbs3,cbs4,interval);
[u_5, mfi_5, qt_5, q_5, R5, p_5]=method5_svd(cbs,cbs2,cbs3,cbs4,interval);
[mfi_6, theta_6, Ruq, u_6, q_6, qt_6, p_6]=method6_uq(cbs,cbs2,cbs3,cbs4,interval);
[u_3,mfi_3,qt_3,q_3,p_3]=method3_geom(interval,cbs,cbs2,cbs4,cbs3);

% calculation of the angle between the theoretical HA (0,0,1) and the estimated HA
[th_ax_1,th_ax_2,th_ax_3,th_ax_4,th_ax_5,th_ax_6]=angle_axis(u_1,u_2,u_3,u_4,u_5,u_6);

% PARAMETERS USED TO EVALUATED THE ERROR BETWEEN THE THEORETICAL HA (NOISY
% FREE) AND THE NOISY FHA
% 1. angle error of the axis vector -> th_ax_a1, ...
% 2. position error of the point p0 -> p_1, p_2 ...
% 3. translation error of q -> qt_1, qt_2, qt_3..

M1(j,:,i)=[th_ax_1 qt_1 p_1 u_1]; % method 1
M2(j,:,i)=[th_ax_2 qt_2 p_2 u_2]; % method 2
M3(j,:,i)=[th_ax_3 qt_3 p_3 u_3]; % method 3
M4(j,:,i)=[th_ax_4 qt_4 p_4 u_4]; % method 4
M5(j,:,i)=[th_ax_5 qt_5 p_5 u_5]; % method 5
M6(j,:,i)=[th_ax_6 qt_6 p_6 u_6]; % method 6

end


end

end
```

SIMULATION - ADDED NOISE IN POSITION

```
function [M1,M2,M3,M4,M5,M6,quantity_translation]= simulation_position_noise(num_sim,
step1)
```

```
%num_sim=1000;
M1=zeros(num_sim,8); %row=number of methods to calculate the HA ; column=parameters to
evaluated the error
M2=zeros(num_sim,8);
M3=zeros(num_sim,8);
M4=zeros(num_sim,8);
M5=zeros(num_sim,8);
M6=zeros(num_sim,8);
[cbs_ideal,cbs2_ideal,cbs3_ideal,cbs4_ideal,RM2_ideal]=simulation(); % ideal movement
(rotation) free noise
% STEP
    %step1=10;
    num_ha=360/step1;
    interval= [1:floor(length(cbs_ideal)/num_ha):length(cbs_ideal)];
    interval=interval(:,floor(length(interval)/8):(floor(length(interval)/8)+1));

cbs_i=cbs_ideal(interval,:); % coordinates point 1
cbs2_i=cbs2_ideal(interval,:); % coordinates point 2
cbs3_i=cbs3_ideal(interval,:); % coordinates point 3
cbs4_i=cbs4_ideal(interval,:); % coordinates point 4
RM2_i=RM2_ideal(:,:,interval); % orientation of the rigid body in space
%points 1, 2, 3 and 4 belong to the rigid body

position=[ 0.05  1  2 ]; % noise levels

for i=1:(length(position)) % 3 levels of noise for the orientation
pos=position(1,i);
for j=1:num_sim

% ADDED ERROR IN POSITION
      mpos=0;
      [error_position]=added_position(cbs_i,pos,mpos); ); % this function creates a
vector of three elements. random gaussian noise. Specific standard deviation, mean=0
      [cbs,cbs2,cbs3,cbs4]=points_error_pos(cbs_i,cbs2_i,cbs3_i,cbs4_i,error_position);
quantity_translation(j)=error_position(3);
interval=[ 1 2 ];


[K_rodri,u_1,theta_1,mfi_1,p_1,q_1,qt_1]=method1_vector(cbs,cbs4,cbs3,cbs2,interval);
[u_2,mfi_2,q_2,p_2,qt_2,RM_m2]=method2_rotmatrix(RM2_i,interval,cbs,cbs2,cbs3,cbs4);
[mfi_4,Om_rodri,theta_4,u_4,p_4,qt_4,q_4]=method4_rodriVirtualBody(cbs,cbs2,cbs3,cbs4,in
terval);
[u_5, mfi_5, qt_5, q_5, R5, p_5]=method5_svd(cbs,cbs2,cbs3,cbs4,interval); % check sign
[mfi_6, theta_6, Ruq, u_6, q_6, qt_6, p_6]=method6_uq(cbs,cbs2,cbs3,cbs4,interval);
%[u_3,mfi_3,qt_3,q_3,p_3]=method3_geom(interval,cbs,cbs2,cbs4,cbs3,u_4);

% calculation of the angle between the theoretical HA and the estimated HA
[th_ax_1,th_ax_2,th_ax_4,th_ax_5,th_ax_6]=angle_axis(u_1,u_2,u_4,u_5,u_6);

% PARAMETERS USED TO EVALUATED THE ERROR BETWEEN THE THEORETICAL HA (NOISY
% FREE) AND THE NOISY FHA
% 1. angle error of the axis vector -> th_ax_a1, ...
```

```
% 2. position error of the point p0 -> p_1, ...
% 3. translation error of q -> qt

M1(j,:,i)=[th_ax_1 qt_1 p_1 u_1]; % method 1
M2(j,:,i)=[th_ax_2 qt_2 p_2 u_2]; % method 2
%M3(j,:,i)=[th_ax_3 qt_3 p_3 u_3]; % method 3
M4(j,:,i)=[th_ax_4 qt_4 p_4 u_4]; % method 4
M5(j,:,i)=[th_ax_5 qt_5 p_5 u_5]; % method 5
M6(j,:,i)=[th_ax_6 qt_6 p_6 u_6]; % method 6

end


end

end
```

FHA ANALYSIS SOFTWARE

```
function FHA_program

[fName,pName] = uigetfile('*','Select a File');
[num,txt,raw] = xlsread(fullfile(pName,fName)); % reads the excel and gets the numeric
as double array, text as cell array and raw data as cell array
rot=num;
basicwaitbar
f = waitbar(0,'Please wait...');
pause(2)
global Rhead
Rhead=zeros(3,3);
j=1;
for i=1:3:length(rot)
    Rhead(:,:,j)=[rot(i,5:7);rot(i,8:10);rot(i,11:13)];
    j=j+1;
end
global t
t=(1:(length(rot)/3))/240;
[x1,y1,z1,x2,y2,z2,x3,y3,z3]=coordinates(rot); % this function get the coordinates of
the sensor attached to the forehead
[xe2,ye2,ze2,Fe2]=changeSRef(x1,y1,z1,x2,y2,z2,x3,y3,z3,rot); % this function changes de
reference system -> thorax
coordi=[xe2' ye2' ze2'];
waitbar(.33,f,'Loading your data');
pause(2)
% run next line to visualize the position (x,y,z) of the sensor during the whole
movement.
%sist reference->breastbone . orientation-> cube reference
[repose]=detection_start(coordi); % this function detect the frame where the movement
starts
repose=270;
global theta  type_mov cb1 cb2 cb3
global cb supermat1
[cb,cb1,cb2,cb3,rcb,vcb,acc,rcbm,vcbm,accm,omega,RG,theta,RGa,vG,aG,w,supermat1
]=rodrigues(xe2,ye2,ze2,rot,repose); % this function calculates kinematic variables
global interval
```

```
[type_mov,interval,neutral,pos_peaks]=divideCycles(w,repose,theta);
% interval-> neutral and extreme points (left and right)
[u,mfi_2,q_2,p_2,qt_2,RM_m2]=methodFHA(Rhead,interval,cb,cb1,cb2,cb3); % it calculates
FHA for each cycle (neutral->extreme, in order to obtain mean FHA)
%
%waitbar(.67,f,'Processing your data');
%pause(2)
%title('FHA between neutral position and extreme position')
% mean FHA. displacement: extreme->neutral; neutral->extreme
global mFHA
[mFHA]=meanFHA(u,type_mov); % this function calculate the mean FHA from all FHAs

ang=10; % angle step. initial position -> final position. FHA . displacement
% From 1st center to 1st extreme:
[cont_total,uFHA,pFHA]=angle_step_FHA(theta,interval,ang,type_mov,Rhead,cb,cb1,cb2,cb3);
% this function divide the movement in displacement depending on the chosen angle step
and calculates the FHA in each displacement
global meanvalangle stdvalangle
[meanvalangle,stdvalangle,valangle]=angle_value(mFHA,uFHA,type_mov); % this function
calculates mean angle and standard deviation of each FHA

waitbar(1,f,'Finishing');
pause(2)

close(f)
ff=figure;
global fv Fe22 head

[fv,Fe22,fvv]=model3d_1(cb,supermat1);

trajectory1point(cb)
global h1
[h1]=display_all_FHA_colors(cont_total,uFHA,pFHA,cb,valangle,stdvalangle);
set(gcf, 'Position', get(0, 'Screensize'));
```

```
sz=size(supermat1);
posize=sz(3);

small_step=1 / (posize - 1);
large_step=2*small_step;
b =
uicontrol('Parent',ff,'Style','slider','Position',[81,54,419,23],'SliderStep',[small_ste
p  small_step],'value',1, 'min',1, 'max',posize,'Position',[493,538,419,23]);

b.Callback=@head_mov;
```

```
% callback to head_mov function when the slider is moved in order to moved the position
of the head
```

```
c = uicontrol(ff,'Style','popupmenu','BackgroundColor',[1.00,1.00,0.07]);
c.FontSize=15;
c.Position = [855,473,60,20];

c.String =
{'1°','2°','3°','4°','5°','6°','7°','8°','9°','10°','15°','20°','30°','40°','50°'};
c.Value=10;
c.Callback = @selection; % call back to selection function when the angle step is
changed
```

```
% PARAMETER 1: mean angle

fprintf('\n\nMean value and standard deviation of angle:  %3.4f ±
%3.4f°\n\n',meanvalangle,stdvalangle)

% PARAMETER 2: area of convex hull
global area_convexx
[area_convexx,inter2d]=cal_area(mFHA,pFHA,uFHA); % this function calculates area of
convex hull
fprintf('\n\nArea of convex hull:  %3.4fcm\n\n',area_convexx)

% PARAMETER 3: mean distance
global md sd
[md,sd]=mean_distance(inter2d); % it calculates mean distance between barycenter and
each intersection
fprintf('\n\nMean distance value and standard deviation:  %3.4f ± %3.4f cm\n\n',md,sd)


title({"MA = "+meanvalangle+" ± "+stdvalangle+"°";  "CH = "+area_convexx+" cm^2"; "MD =
"+md+" ± "+sd+" cm"},'FontSize', 20)

end
```